JCI insight

Tnfrsf4-expressing regulatory T cells promote immune escape of chronic myeloid leukemia stem cells

Magdalena Hinterbrandner, … , Adrian F. Ochsenbein, Carsten Riether

JCI Insight. 2021. https://doi.org/10.1172/jci.insight.151797.

Research In-Press Preview Hematology Stem cells

Graphical abstract

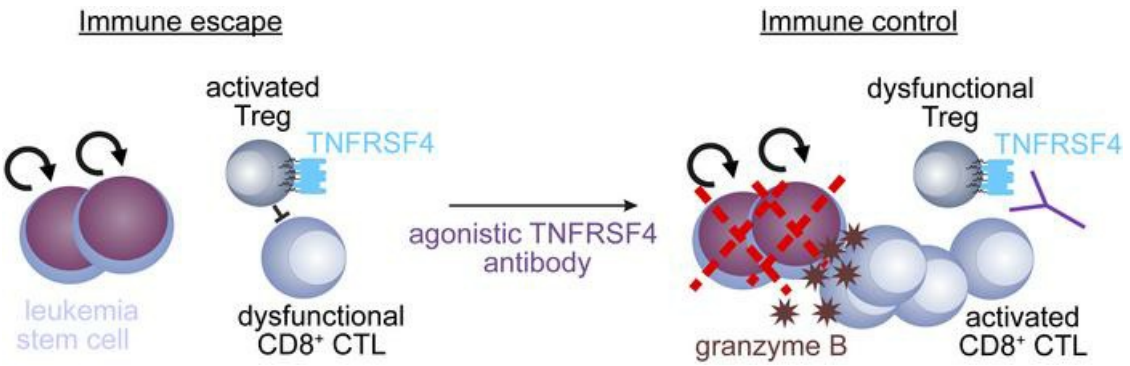

Tnfrsf4-expressing regulatory T cells promote immune escape of chronic myeloid leukemia stem cells.

Magdalena Hinterbrandner[1,2,3,†], Viviana Rubino[1,2,3†], Carina Stoll[1,2], Stefan Forster[1,2,3], Noah Schnüriger[1,2,3], Ramin Radpour[1,2], Gabriela M. Baerlocher[2,4], Adrian F. Ochsenbein[1,2] and Carsten Riether[1,2,*]

[1]Department of Medical Oncology, Inselspital, Bern University Hospital, University of Bern, Switzerland

[2]Department for BioMedical Research (DBMR), University of Bern, Bern, Switzerland

[3]Graduate School of Cellular and Biomedical Sciences, University of Bern, Bern, Switzerland

[4]Department of Hematology and Central Hematology Laboratory, Inselspital, Bern University Hospital, University of Bern, Switzerland.

***Corresponding author:** Carsten Riether, Department of Medical Oncology, Inselspital, Bern University Hospital, University of Bern, Switzerland; E-Mail: carsten.riether@insel.ch, Telephone: +41-31-632-0956, Fax: +41-31-632-3297, ORCID: https://orcid.org/0000-0001-7512-513X.

† Authors contributed equally to the work.

Conflict of interest statement: The authors declare no competing financial interests related to this study.

Abstract

Leukemia stem cells (LSCs) promote the disease and seem resistant to therapy and immune control. Why LSCs are selectively resistant against elimination by cytotoxic $CD8^+$ T cells (CTLs) is still unknown. In this study, we demonstrate that LSCs in chronic myeloid leukemia (CML) can be recognized and killed by $CD8^+$ CTLs in vitro. However, Tregs, which preferentially localized close to $CD8^+$ CTLs in CML bone marrow (BM), protected LSCs from MHC-class I dependent $CD8^+$ CTL-mediated elimination in vivo. BM Tregs in CML were characterized by the selective expression of tumor necrosis factor receptor 4 (Tnfrsf4). Stimulation of Tnfrsf4-signaling did not deplete Tregs but reduced the capacity of Tregs to protect LSCs from $CD8^+$ CTL-mediated killing. In the BM of newly diagnosed CML patients, *TNFRSF4* mRNA levels were significantly increased and correlated with the expression of the Treg-restricted transcription factor *FOXP3*. Overall, these results identify Tregs as key regulator of immune escape of LSCs and TNFRSF4 as a potential target to reduce the function of Tregs and boost anti-leukemic immunity in CML.

Introduction

BCR-ABL1 Tyrosine kinase inhibitors (TKI) have revolutionized the clinical management of chronic myeloid leukemia (CML) patients. These TKIs remarkably improved the prognosis of CML patients as indicated by the induction of durable complete cytogenetic hematologic responses in the majority of patients and even deep molecular remissions in a proportion of patients (1–3). Only half of the latter patients can permanently discontinue TKI therapy and maintain a treatment-free remission (4). This is due to the insufficient action of TKIs on quiescent, self-renewing leukemia stem cells (LSCs) in the bone marrow (BM) of the patients. Such persistent LSCs can maintain the disease and are responsible for relapse of the disease upon drug discontinuation (5).

Immunotherapy may be a potential approach to eradicate such TKI-insensitive cells/LSCs in CML patients. Leukemia cells including LSCs are sensitive to lysis by T cells and NK cells. The relevance of allo-reactive $CD8^+$ T cells in the control of leukemia has impressively been documented in leukemia patients receiving allogenic hematopoietic stem cell transplantation (aHSCT)(6–8) or in patients receiving donor lymphocyte infusions after relapse (7, 9, 10). However, the contribution of the endogenous adaptive immune system to the pathophysiology of leukemia is less evident. Recent studies using highly sensitive detection methods for the BCR-ABL1 transcript demonstrated that residual leukemic cells and CML LSCs can be detected even in patients who are in a molecular remission after TKI discontinuation (11, 12). These findings suggest that the host immune system may contribute to the control of these residual cells and prevent CML progression/relapse in these patients.

Compared to the majority of solid tumors, CML cells have a low mutational burden resulting in the generation of only a limited number of neo-antigens that may be detected by specific cytotoxic $CD8^+$ T cells (CTLs) (13). As yet, endogenous $CD4^+$ and $CD8^+$ T cell responses directed against leukemia-specific (LSA) and leukemia-associated antigens have been detected in chronic phase CML patients (14–17). Especially LSA derived from the junctional region of BCR-ABL1, which represent CML-specific neo-antigens, but also aberrantly expressed self-proteins such as WT-1, PR and hTERT have been shown to be immunogenic and to elicit specific T cell responses in vitro and in vivo (14, 16, 17). However, despite the expression of major histocompatibility complex I and II (MHC class I and II) and co-stimulatory ligands on LSCs which allow their interaction with $CD4^+$ and $CD8^+$ T cells (18–20), activated CTLs fail to eliminate LSCs in vivo and rather promote their expansion (18, 19, 21). This raises the hypothesis that the BM microenvironment may harbor immunosuppressive mechanisms that prevent the immune control of LSCs.

Regulatory T cells (Tregs) are essential for the maintenance of immune tolerance and are a crucial component of the BM microenvironment during homeostasis and in leukemia (22, 23). Numbers and frequencies of Tregs in peripheral blood and BM are increased in CML patients at diagnosis (23–26). Furthermore, Tregs are reduced especially in patients who achieved a complete cytogenetic response (27). Similarly, a successful maintenance of treatment-free-remission is associated with reduced numbers of Tregs (28–30). How Tregs are involved in the development of CML and immune escape of LSCs is, however, still unknown.

In this study, we analyzed the contribution of BM Tregs in the pathogenesis of CML. We show that regulatory T cells protect LSCs from elimination by cytotoxic $CD8^+$ CTLs and that this process can be successfully inhibited by activation of Tnfrsf4-signaling on Tregs. Overall, this

study reveals TNFRSF4 as a potential target to reduce the function of Tregs and improve anti-leukemic immunity against LSCs.

Results

Thymic-derived Tregs with an activated immunophenotype accumulate in the BM of CML mice.

We first analyzed spatial distribution of BM Tregs in respect to CTLs as well as Treg numbers and phenotype in a murine retroviral transduction/transplantation CML model (31). In the BM of CML and naïve mice, Tregs were widely distributed, did not form clusters and were preferentially localized near to CTLs as analyzed by immunohistochemistry (IHC) **(Figure 1A-D)**.

FACS analysis revealed that absolute numbers of Tregs and the frequency of Treg cells among $CD4^+$ T cells in the BM of CML mice were significantly increased compared to BM of naive mice **(Figures 1E, S1A, B).** In addition, the frequency of Treg cells among $CD4^+$ T cells correlated with leukemia burden (**Figure 1F**). The apoptosis rate of $CD4^+$ T cells in the BM of CML mice was substantially higher in BM of than naïve control mice. However, the apoptosis rate was similar in Tregs and conventional $CD4^+$ T cells (Tconv) (Annexin V^+ cells; Tregs CML: 23.87±3.67 and Tconv CML: 22.81±7.45) and thus cannot explain the increased frequency of Tregs in total $CD4^+$ T cells **(Figure 1G)**. In contrast, Ki-67 staining indicated an enhanced proliferation of Treg cells (**Figure 1I**). To determine the cellular origin of Tregs in CML, we stained for Helios and neuropilin-1, two markers which allow to discriminate Tregs which develop in the thymus (tTregs) and Tregs which arise by conversion from conventional $CD4^+Foxp3^-$ T cells in peripheral tissues (pTregs) (32). The BM of CML mice harbored a greater proportion of tTregs **(Figure 1J)**. In addition, Tregs in the BM of CML mice had an

activated effector phenotype (eTregs) compared to controls as indicated by an increased expression of CD44 and lack of CD62L expression on the cell surface **(Figure 1K).**

The accumulation of eTregs was further confirmed by assessing markers which are characteristically increased in expression during the differentiation from naive/resting Tregs (nTregs) into eTregs and which mediate their immunosuppressive function such as the transcription factor Foxp3 and the surface molecules cytotoxic T-lymphocyte-associated protein 4 (Ctla-4), glucocorticoid-induced TNFR-related protein (Gitr), glycoprotein-A repetitions predominant (Garp) and transforming growth factor β1 (Tgf-β1) (**Figure 1L-O**). Importantly, these phenotypic changes observed in the BM of CML mice were not observed in lymphoid organs such as the spleen **(Figures S1C-H)**.

Tregs in the BM of CML mice display an activated and immunosuppressive gene expression signature.

Next, we performed an RNA sequencing (RNA-Seq) analysis on Tregs isolated from BM of naïve and CML mice. In the principal component analysis (PCA) analysis, Tregs isolated from naive mice clustered together **(Figure 2A)**. In contrast, Tregs derived from the BM of CML mice showed a certain degree of heterogeneity in terms of gene expression (PC2). Independent of this heterogeneity, Tregs derived from CML mice clearly separated from naïve Tregs (PC1). RNA-Seq analysis identified 639 genes which were differentially expressed between the two groups **(Figure 2B, Supplementary Table 1).** 460 genes were upregulated, and 179 genes were downregulated. Gene ontology (GO) analysis assigned the 639 differently expressed genes mainly into 12 different GO categories **(Figure 2C)**. The differentially expressed genes were primarily involved in signaling pathways related to cell metabolism, cell cycle, negative regulation of T cell proliferation and cytokine production. Overall, these results indicate a BM-specific accumulation of eTregs in CML mice.

Depletion of Tregs eliminates LSCs and leads to long-term survival of CML mice.

To study the functional relevance of Tregs in CML development in vivo, we depleted Tregs in *Foxp3*^{DTR} CML mice by administration of diphtheria toxin (DT) (33). *Foxp3*^{DTR} CML mice with comparable leukemia burden (37±8 BCR-ABL1-GFP$^+$Gr-1$^+$ granulocytes (L-Gr-1$^+$ cells)/µl blood) were randomized to control treatment with vehicle or DT for Treg depletion thirteen days after leukemia transplantation **(Figure 3A)**. DT treatment resulted in the reduction of L-Gr-1$^+$ cells in peripheral blood and long-term survival **(Figure 3B and data not shown)**. In contrast, PBS-treated *Foxp3*^{DTR} CML mice all died within 30 days. No residual BCR-ABL1-GFP$^+$ cells could be detected in blood, spleen and BM of DT-treated *Foxp3*^{DTR} CML mice by FACS 90 days after transplantation **(data not shown)**. These findings indicate that LSCs were either eliminated or effectively controlled by the depletion of Tregs. To determine residual disease with the most sensitive assay, we transplanted BM cells of surviving primary DT-treated *Foxp3*^{DTR} CML mice into lethally irradiated secondary BL/6 recipients. All secondary recipients survived up to 90 days without any signs of leukemia **(Figure 3C)**.

To address whether LSCs are indeed affected by depletion of Tregs in our model in more detail, leukemia bearing *Foxp3*^{DTR} mice were treated as described above with DT and animals were sacrificed 21 days after leukemia induction. DT treatment successfully reduced/depleted Tregs in the BM of CML mice. (**Figure 3D**). Leukemia burden as indicated by smaller spleen size, lower numbers of L-Gr-1$^+$ cells in blood and leukemic lin$^-$ and progenitor cells in the BM was lower in DT CML mice compared with control CML mice **(Figures 3E-H)**. Furthermore, Treg depletion significantly reduced LSC numbers and resulted in fewer BCR-ABL1-GFP$^+$ colonies formed in methylcellulose from lin$^-$ BM cells **(Figures 3I, J)**. To functionally investigate whether leukemia-initiating cells had been eradicated, we transferred BM cells from primary CML into lethally irradiated secondary recipient mice. All secondary recipients transplanted with BM from PBS-treated primary CML developed the disease and succumbed to it with a median latency of approximately 32 days. In contrast, secondary recipients receiving BM from

Treg-depleted primary CML mice survived long-term without signs of leukemia as analyzed by FACS of peripheral blood, BM and spleen 90 days after transplantation **(Figure 3K and data not shown)**. Similar results on the immunophenotype of Tregs in the BM and the contribution of Tregs to leukemia development were obtained in a blast crisis CML model **(Figure S2).** Overall, these results indicate that Treg depletion in a therapeutic setting contributes to the elimination of leukemia-initiating cells in vivo in mice.

$CD8^+$ CTLs selectively eliminate CML LSCs by secretion of perforin in vitro and in vivo. Next, we determined whether Tregs directly regulate LSCs in CML or whether they constrain anti-leukemic $CD8^+$ T cell immunity and thereby promote immune escape of LSCs. Therefore, we first addressed whether $CD8^+$ CTLs from the BM of CML mice have the capacity to recognize and kill LSCs. We co-incubated FACS-purified LSCs with $CD8^+$ CTLs derived from the BM of CML-bearing mice overnight followed by plating in methylcellulose. Co-incubation of LSCs with $CD8^+$ CTLs resulted in the generation of significantly fewer colonies in primary platings **(Figure 4A** and **Figure S3A**). The effect on fewer colony formation was maintained in re-plating experiments performed in the absence of $CD8^+$ CTLs. Killing of LSCs by $CD8^+$ CTLs was dependent on MHC I expression on LSCs **(Figure S3B).** In contrast, $CD8^+$ CTLs isolated from the BM of naïve did not affect clonogenicity of LSCs (data not shown). Overall, these data suggest that BM $CD8^+$ CTLs have the capacity to kill LSCs in vitro.

The accepted hallmark of a fully active $CD8^+$ CTL remains its perforin killing machinery, even though they exhibit both Fas ligand (FasL)-based and perforin-based lytic activities (34). To investigate if BM $CD8^+$ CTLs reduce LSCs through perforin-mediated killing in CML, we co-incubated LSCs in the presence of $CD8^+$ CTLs derived from the BM of perforin-proficient and -deficient CML mice. In contrast to co-incubation with perforin-proficient $CD8^+$ CTLs, co-incubation with perforin-deficient CML $CD8^+$ CTLs did not reduce colony formation **(Figure**

4B). Similarly, the exposure of LSCs to the granzyme B inhibitor I prior to co-culture with $CD8^+$ CTLs protected LSCs from $CD8^+$ CTLs -mediated killing in vitro **(Figure S3B)**. Importantly, the clonogenic potential of normal lineage-negative c-$kit^+$$sca\text{-}1^+$ hematopoietic stem/progenitor cells (LSKs) derived the BM of naïve BL/6 mice was not affected by co-incubation of LSKs with $CD8^+$ CTLs from CML mice **(Figure S3C)**.

Lastly, we induced CML in BL/6 and perforin-deficient mice (BL/6 CML and *Prf*$^{-/-}$ CML, respectively, **Figure 4C**). 15 days after leukemia induction, mice were sacrificed, and BM and spleens were analyzed. *Prf*$^{-/-}$ CML mice had an increased leukemia burden as indicated by bigger spleen size, higher numbers of BCR-ABL1-GFP^+ leukemia splenocytes (L-splenocytes) and of BCR-ABL1-GFP^+ lineage-negative (L-lin^-) cells in the BM compared to BL/6 CML mice **(Figures 4D-F)**. Similarly, we found a strong increase in LSC numbers in the BM of *Prf*$^{-/-}$ CML mice **(Figure 4G)**. LSCs can be further sub-divided into long-term (LT-)LSCs, leukemia multipotent progenitors (L-MPPs) and leukemia progenitor cells (L-HPC-1s and L-HPC-2s) using the markers CD150 and CD48 (18, 35). Phenotypic LSC subsets analysis revealed that the increase of LSCs in *Prf*$^{-/-}$ CML mice was in great part mediated by a significant accumulation of L-HPC-2 cells and more importantly of disease-initiating and -maintaining LT-LSCs **(Figures 4H-L)**. Animals transplanted with BM from *Prf*$^{-/-}$ CML mice in secondary transplantation experiments succumbed to the disease significantly faster than mice transplanted with BM from BL/6 control CML mice **(Figure 4M)**. Overall, these data suggest that cytotoxic $CD8^+$ T cells can recognize and eliminate CML LSCs.

Tregs protect LSCs from $CD8^+$ CTL-mediated killing in vitro and in vivo.

To prove that Tregs in the BM constrain anti-leukemic $CD8^+$ T cell immunity in CML, *Foxp3*^{DTR} CML mice were treated 13 days after CML induction with either PBS, DT, a depleting αCD8 mAb (PBS/αCD8) alone or in combination (DT/αCD8) (**Figure 5A**).

Depletion of $CD8^+$ T cells alone did not affect leukemia load in the spleen (**Figure 5B**). Similarly, numbers of L-lin^- cells, L-c-kit^{high} cells and LSCs in the BM were comparable to PBS-treated control CML mice after $CD8^+$ T cell depletion (**Figures 5C-E).** In line with the findings depicted in Figure 2, Treg depletion by DT administration considerably reduced leukemia load and LSC numbers in the BM (**Figures 5C-E, Figure S4A**). In contrast, DT/αCD8 treatment restored leukemia burden and LSC numbers in BM to comparable levels as PBS and αCD8/PBS-treated CML mice. These findings were confirmed functionally by secondary transplantation experiments (**Figure 5F**).

Similarly, co-culture experiments revealed that $CD8^+$ CTLs fail to eliminate LSCs in vitro in the presence of Tregs derived from the BM of CML but not from naïve mice **(Figure S3D)**. In addition, co-incubation with CML Tregs alone did not alter the clonogenic potential of LSCs in vitro.

Lastly, we investigated whether BM $CD8^+$ CTLs from DT-treated CML mice are more potent in eliminating LSCs in vitro. Thus, we co-cultured LSCs with BM $CD8^+$ CTLs from naive mice and PBS- or DT-treated CML mice overnight followed by plating in methylcellulose. Co-incubation of $CD8^+$ CTLs from DT-treated CML mice even further reduced the clonogenic potential of LSCs than $CD8^+$ CTLs from PBS-treated CML mice **(Figure 5G).** In addition, the expression of genes related to the capacity of $CD8^+$ CTLs to lyse and kill LSCs such as *GrzmA* and *GrzmB* were significantly increased in $CD8^+$ CTLs derived from DT-treated CML mice compared to $CD8^+$ CTLs from PBS-treated CML mice **(Figures 5H-J).** These data suggest that Tregs in the BM indirectly promote immune escape of LSCs through modulation of $CD8^+$ CTL activity.

Tregs in CML are activated by antigens presented on MHC class II-expressing LSCs.

The expression of cognate antigens triggers the differentiation of tTregs (36–38). To determine whether leukemia cells and especially LT-LSCs have the capacity to interact with and activate Tregs via MHC class II/TCR interaction, we assessed the expression of MHC class II on LSC subsets and more differentiated leukemia and progenitor cells by FACS. MHC class II was strongly expressed on LSC subsets including LT-LSCs. In contrast, leukemia progenitor and fully differentiated L-Gr-1^{+} cells had reduced levels of MHC class II expressed on the cell surface **(Figure S4B).** These results indicate that especially LSCs possess the capacity to interact and activate tTregs in our CML mouse model.

To address whether a lack of MHC class II on LSCs affects Treg activation and consequently disease development in our CML model, we transplanted MHC class II (*H2*) -proficient and -deficient BCR-ABL1-GFP-transduced LSKs into non-irradiated *Foxp3*^{DTR} mice. Even though *H2*$^{-/-}$ and BL/6 LSCs did not differ in their potential to form colony in primary and secondary replating experiments in vitro (**Figure S4C**), leukemia developed significantly slower in *H2*$^{-/-}$ CML mice compared to BL/6 CML mice as indicated by considerably lower levels of L-Gr-1^{+} cells in peripheral blood (**Figure 6A**). Eighteen days after leukemia induction, CML mice of both groups were sacrificed, and spleen and BM were analyzed. Spleen size was significantly smaller in *H2*$^{-/-}$ CML mice compared to controls, indicating a lower leukemia burden in these mice (**Figure 6B**). Phenotypic analysis of lin^{-} BM cells by FACS further revealed significantly fewer L-lin^{-} and L-c-kit^{high} cells and a 7-fold reduction of LSCs in *H2*$^{-/-}$ CML mice (**Figures 6C-E**), a finding that was functionally confirmed by colony assays of lin^{-} BM cells in vitro (**Figure 6F**). To verify that the decrease in LSCs detected by FACS analysis and in colony forming assays in vitro represents a reduction in cells that can induce leukemia in vivo, we secondarily transplanted BM cells from primary BL/6 and *H2*$^{-/-}$ CML mice into lethally irradiated secondary BL/6 recipient mice. Mice that received BM from BL/6 leukemia mice developed a more severe course of the disease and died with a median latency of 29 days. In

contrast, mice which were transplanted with BM cells from primary *H2*$^{-/-}$ CML mice survived long-term without any signs of leukemia **(Figure 6G).**

Analysis of the activation state of Tregs in the BM of primary BL/6 and *H2*$^{-/-}$ CML mice revealed fewer eTregs in the BM of CML mice in the absence of MHC class II expression on LSCs. Importantly, the frequency of eTregs in these mice was comparable to the eTreg frequency in the BM of naive mice (**Figure 6H, I**). The reduced activation of Tregs in *H2*$^{-/-}$ CML was complemented by a significant increase in the frequency and absolute numbers of CD8^{+} T cells (**Figure 6J, K**).

CD8^{+} CTL depletion renders *H2*$^{-/-}$ CML mice susceptible to disease development.

Based on these results, we speculated that blockade of CD8^{+} CTL activity or depletion of CD8^{+} T cells would render *H2*$^{-/-}$ CML mice susceptible to CML development. To test this hypothesis, we depleted CD8^{+} CTLs in *H2*$^{-/-}$ CML mice by repetitive treatment with an αCD8 mAb (**Figure 6L**). While IgG-treated control *H2-/-* CML mice were protected from CML development and survived long-term, CD8^{+} CTL depletion completely restored the competence of *H2*$^{-/-}$ CML mice to develop leukemia and resulted in death of the mice approximately 20-30 days after transplantation (**Figure 6M, N**). To further determine the effect of CD8 blockade on LSCs in *H2*$^{-/-}$ CML, αCD8 mAb- or control IgG-treated *H2*$^{-/-}$ CML mice were sacrificed 16 days after CML induction and BM was analyzed. CD8^{+} CTL depletion significantly increased leukemia burden as demonstrated by an elevated number of L-lin^{-} cells and LSCs as assessed phenotypically by FACS and functionally by colony formation assays and secondary transplantation of BM into secondary recipients (**Figure 6O-R**). These results indicate that Tregs are activated by antigens presented on MHC class II-expressing leukemia cells and LSCs.

Stimulation of Tnfrsf4-signaling reduces the capacity of Tregs to protect LSCs from CD8^{+} CTL- mediated killing in CML.

Next, we determined whether immune-related surface receptors which were up-regulated in CML BM could be used to selectively target Tregs. Among the most up-regulated genes, our RNA-seq analysis identified five immune-related surface receptors (*Tnfrsf1b, Tigit, Tnrsf4, Tnfrsf8, and Tnfrsf9,* **Supplementary Table 1**). Because *Tnfrsf1b* and *Tnfrsf9* have a reported role in the regulation of normal hematopoietic stem cells (39) and myeloid differentiation of early hematopoietic progenitor cells (40, 41), we focused our subsequent analysis on *Tigit*, *Tnrsf4* and *Tnfrsf8*. FACS analysis revealed that besides $CD4^+Foxp3^+$ Tregs also a fraction of $CD8^+$ CTLs, $CD4^+Foxp3^-$ T cells, L-Gr-1^+ cells and LSCs express Tigit in the BM of CML mice (**Figure S4C, D**). In contrast, Tnfrsf8, alias CD30, was absent on protein level on all cell populations analyzed including $CD4^+$ $Foxp3^+$ Tregs (**data not shown**). Tnfrsf4 could not be detected on the surface of $CD8^+$ T cells, L-Gr-1^+ cells and LSCs, while a substantial fraction of $CD4^+Foxp3^+$ Tregs and a minor fraction of $CD4^+Foxp3^-$ T cells expressed Tnfrsf4 in the BM of CML mice **(Figure 7A, B)**. These data suggest that Tnfrsf4 may serve as a target to selectively eliminate/inactivate Tregs in CML without directly affecting $CD8^+$ CTL-mediated immunity and leukemia cells. To proof this concept, we co-cultured LSCs and $CD8^+$ CTLs from CML BM in the presence and absence of CML Tregs and an agonistic Tnfrsf4 antibody followed by plating in methylcellulose. The agonistic Tnfrsf4 antibody OX86 has been shown to mediate Tnfrsf4 forward signaling on Tregs leading to their functional inactivation in vitro and in vivo (42–44) and has also been demonstrated to deplete Tnfrsf4-expressing Tregs in other solid tumor models (45). $CD8^+$ CTLs reduced colony formation of LSCs independent of the presence of the antibody. In contrast, addition of the antibody to the co-culture of LSCs, Tregs and $CD8^+$ CTLs reduced colony formation of LSCs to comparable levels as co-cultures of LSCs and $CD8^+$ CTLs. Colony formation of LSCs was not affected by addition of the antibody into the monoculture **(Figure 7C).**

To demonstrate the in vivo relevance of our findings, BL/6 CML mice were treated with either control IgG or an agonistic Tnfrsf4 antibody starting at day 12 day after CML induction and disease development was monitored. Tnfrsf4 antibody treatment reduced L-Gr-1$^+$ cells in the peripheral blood and significantly prolonged survival of CML mice with 60% of mice surviving long-term (**Figure 7D, E**). Mechanistically, Tnfrsf4 antibody treatment significantly increased the CD8/Treg ratio in BM without depletion/reducing Treg numbers (**Fig. 7F, G**) which resulted in reduced leukemia and reduced numbers of BM LSCs (**Fig. 7H-J**). Overall, these data indicates that blockade of TNFRS4-signaling on Tregs promotes anti-leukemic immunity and promotes elimination of CML LSCs by CD8$^+$ CTLs.

Tregs protect primary human CD34$^+$CD38$^-$ CML stem/progenitor cells from CD8$^+$ CTL-mediated killing in vitro.

To validate the significance of our findings for human CML, we addressed whether cytotoxic CD8$^+$ T cells can kill CD34$^+$CD38$^-$ CML stem/progenitor cells derived from newly diagnosed chronic phase CML patients and whether this effect can be reverted in the presence of Tregs **(Table S2)**. Therefore, we first co-incubated FACS-purified CML stem/progenitor cells overnight with FACS-purified CD8$^+$ CTLs derived from the same patients at an effector to target ratio of 1:1, followed by plating in methylcellulose. Like our results obtained with mice, co-incubation with CD8$^+$ CTLs reduced the clonogenic potential of primary CML stem/progenitor cells in a granzyme-dependent manner **(Figures 8A, B, Table S2)**. Importantly, addition of Tregs to the culture of CD8$^+$ CTLs and CML stem/progenitor cells prevented elimination of CML stem/progenitor cells by CD8$^+$ CTLs **(Figure 8C)**. In contrast, co-culture of LSCs with Tregs did not affect their clonogenic potential. Overall, these data indicate that Tregs in the BM protect LSCs from elimination by CD8$^+$ CTLs in CML.

Tregs are increased in BM of newly diagnosed CML patients and are located close to $CD8^+$ CTLs.

In line with previous findings (23), analysis of BM sections from a limited number of CML patients and healthy donors by IHC demonstrated that Treg numbers tend to be increased in CML BM **(Figure 8D)**. Tregs were widely distributed in the BM parenchyma in CML and healthy conditions **(Figure 8E and Figure S5A**). While a comparable frequency of about 30% Tregs were found close to normal $CD34^+$ stem/progenitor cells and $CD8^+$ CTLs in the healthy donor BM (**Figure S9B-D**), the majority of Tregs in BM of CML patients were close to $CD8^+$ CTLs (58,44 ± 6.53%) but not $CD34^+$ CML stem/progenitor cells (18,33 ± 3.87%) **(Figure 7F-H)**

***TNFRSF4* mRNA expression is increased in the BM of CML patients.**

To demonstrate a role for TNFRSF4 in CML, we analyzed mRNA expression of *TNFRSF4* and Treg-associated genes such as *FOXP3* and *TGFB1* in the BM of 66 newly diagnosed chronic phase CML patients and 73 healthy controls using a publicly available microarray dataset (GSE13159). We found the expression of *TNFRSF4*, *FOXP3* and *TGFB1* mRNA significantly increased in BM samples from CML patients compared to controls (**Figures 8I-K**). Importantly, the expression of *FOXP3* mRNA strongly correlated with *TNFRSF4* and *TGFB1* in the BM of CML patients but not in healthy donor control BM (**Figures 8L, M and Figure S5E, F**). FACS analysis of the BM from a limited number of newly diagnosed CML patients revealed that a significant fraction of $CD4^+CD127^{lo}CD25^+$ BM Tregs express the TNFRSF4 on the surface whereas TNFRSF4 was absent on $CD8^+$ T cells and CML stem/progenitor cells **(Figure 8N and Figure S5G)**.

Discussion

Leukemia can only be eradicated long-term by targeting disease-initiating and -maintaining LSCs (5, 46). Despite the clinical success of TKIs in the treatment of CML patients, quiescent, TKI-resistant LSCs remain in the BM in a majority of patients and can cause relapse of the disease after drug discontinuation or through the acquisition of mutations (5). For these patients, immunotherapy might be a potential therapeutic option. However, LSCs also seem resistant to elimination by activated $CD8^+$ CTLs in vivo and various immune effector mechanisms contribute to the expansion of LSCs rather than to their elimination (18, 19, 47, 48). Why LSCs are selectively resistant against elimination by $CD8^+$ CTLs is still unknown.

In the present study, we describe Tregs in the BM as an important mediator of immune escape of LSCs in CML. During homeostasis, Tregs are enriched in the BM and are thought to provide an immune-privileged niche, protecting hematopoietic stem and progenitor cells (HSPCs) from immune destruction (22). In addition, Camacho et al. recently demonstrated that BM Tregs regulate hematopoiesis indirectly through modulation of stromal cell function (49). In CML, numbers and frequencies of Tregs in peripheral blood and BM are increased in patients at diagnosis and correlate with a poor prognosis (Sokal score) (23–26). In addition, Treg numbers further increase in accelerated phase and blast-crisis CML patients compared to chronic phase CML patients (25). In line with these findings, we document that Tregs are increased in CML BM in frequency and absolute numbers in a murine CML model. Depletion of Tregs in a therapeutic setting through short-term administration of DT in *Foxp3*^{DTR} mice resulted in activation of $CD8^+$ CTLs, elimination of LSCs and long-term survival. In addition, co-culture of Tregs from the BM of CML mice but not from BM of naïve mice with LSCs and $CD8^+$ CTLs prevented the killing of LSCs in vitro. The results obtained in mice were confirmed in comparable experiments using Treg, CML stem/progenitor cells and $CD8^+$ CTLs from newly diagnosed CML patients and suggest a similar role of Treg in the protection of LSCs from $CD8^+$ CTLs mediated killing in humans.

Our study describes the distribution and the spatial localization of Tregs in the BM during homeostasis and in CML. Tregs were widely distributed throughout the BM parenchyma in mice and humans. In human CML, the majority of Tregs were localized close to $CD8^+$ CTLs and not close to $CD34^+$ CML stem/progenitor cells. Similarly, a big proportion of Tregs were in close proximity to $CD8^+$ CTLs in the BM of CML mice. Overall, our findings suggest that Tregs in CML BM preferentially interact with $CD8^+$ CTLs and regulate their function instead of interacting directly with CML stem/progenitor cells, findings, which are supported by functional data generated in this study.

Tregs in CML BM were activated, thymic-derived and over-expressed receptors such as Ctla-4, Gitr, Garp and Tgf-β1 on the surface which have been previously reported to mediate their activity and immunosuppressive function in various cancer entities (50). Given that TCR stimulation is required for activation and acquisition of suppressive function in Treg cells (36–38), the activated profile of BM Tregs in our study suggests that antigen stimulation may play an important role in the activation and accumulation of Treg cells in CML BM. In line with this hypothesis, we found that MHC class II expression on LSCs promoted the activation and accumulation of eTregs in the BM resulting in immune escape of LSCs from $CD8^+$ CTL-mediated immunity in CML. In CML patients, leukemia-antigen specificity of $CD4^+$ T cells has been documented in several independent studies (17, 51–53). However, whether CML-antigen specific Tregs are part of this $CD4^+$ T cell population is still unclear. In general, the evidence for functional tumor-antigen specific Tregs in cancer is very weak due to the lack of adequate MHC class II tetramers and antigen-specific Treg cells have only been documented in few solid tumors and in B acute lymphoblastic leukemia (54–58).

CML has a lower mutational burden as most solid tumors and has therefore a lower number of neoantigens that can be recognized by specific $CD8^+$ CTLs (59), suggesting that LSCs in

myeloid leukemia may have a low degree of immunogenicity. Similarly, the frequency of CML-specific $CD8^+$ CTLs at diagnosis in humans is rather low (14, 60). Here, we document for the first time that CML LSCs can be recognized and killed by antigen-specific BM $CD8^+$ CTLs through perforin/granzyme-mediated lysis, even though only a minority of the BM $CD8^+$ CTLs are leukemia-specific.

In contrast, $CD8^+$ CTLs may also contribute to the expansion of LSCs as documented in earlier studies (18, 19, 47, 48). This discrepancy may be explained by differences in the activation status of the specific T cells, the effector:target ratio and, as shown in our present study, the presence of Tregs (18, 19, 47, 48). For example, the transfer of a large numbers of activated T cell receptor transgenic T cells leads to a IFNγ-dependent expansion of LSCs, whereas the physiological activation of few CML-specific $CD8^+$ T cells leads to the elimination of LSCs (19).

Tregs are an important regulator of homeostasis in the BM and provide an immune privilege niche for HSCs (49, 61). Due to the crucial role of Tregs in the regulation of BM microenvironment unselective targeting of Tregs would seriously affect normal hematopoiesis. To identify surface markers that can be selectively targeted on Tregs in the BM of CML mice, we performed an RNA-Seq analysis of BM Tregs from CML and naïve mice. In line with our phenotypic observations, Tregs in the BM of CML mice had an enhanced expression of genes related to Treg differentiation and function, cell cycle, inflammation and immunosuppression. We identified the TNFRSF4 as a cell surface receptor which was highly overexpressed on CML Tregs at mRNA level. Activation of TNFRSF4 forward signaling by the agonistic antibody OX86 did not deplete Tregs but reduced the immunosuppressive function of Tregs and thereby inhibited the capacity of BM Tregs to protect LSCs from elimination by $CD8^+$ CTLs. TNFRSF4 agonists are currently being investigated alone or in combination with other immunotherapies for the treatment of various tumor entities. TNFRSF4 agonists are currently being investigated

alone or in combination with other immunotherapies for the treatment of various tumor entities (50). Consequently, the efficacy of an agonistic TNFRSF4 antibody to modulate T cell-immunity and to eliminate LSCs in CML patients could be directly addressed in patients who did not obtain a deep molecular remission as well as in patients who relapsed after TKI stop. In summary, our study identifies Tregs as a central regulator of immune escape of LSCs and TNFRSF4 as a potential target to modulate the Tregs and promote anti-leukemic immunity in CML.

Methods

Antibodies for flow cytometry

Mouse: αLy-6A/E-PerCP-Cy5.5 (Sca-1, clone D7; 1:600, Cat# 108123, RRID:AB_893619), αCD117-APC-Cy7 (c-kit, clone 2B8; 1:300, Cat# 105838, RRID:AB_2616739), αLy6G/C- PE (clone RB6-8C5, 1:400, Cat# 108408, RRID:AB_313373), αCD19-APC-Cy7 (clone 6D5, 1:300, Cat# 115530, RRID:AB_830707), αCD4-BV650 (clone RM4-5, 1:600, Cat# 100555, RRID:AB_2562529), αCD150-PE (clone TC15-12.F12.2, 1:200, Cat# 115903, RRID:AB_313682), αCD48-AlexaFluor700 (clone HM48-1, 1:100, Cat# 103426, RRID:AB_10612755), αCD16/32-PE-Cy7 (clone 93, 1:400, Cat# 101307, RRID:AB_312806), αCD4-PE-Cy7 (clone GK1.5, 1:600, Cat# 100421, RRID:AB_312706), αCD8-AlexaFluor700 (clone 53-6.7, 1:800, Cat# 100729, RRID:AB_493702), αCD4-APC-Cy7 (clone GK1.5, 1:600, Cat# 100414, RRID:AB_312699), αCD8-PE-Cy7 (clone 53-6.7, 1:600, Cat# 100721, RRID:AB_312760), αCD25-PerCP-Cy5.5 (clone PC61, 1:300, Cat# 102030, RRID:AB_893288), αHelios-AlexaFluor647 (clone 22F56, 1:40, Cat# 137208, RRID:AB_10552902), Armenian hamster IgG-AlexaFluor647 (clone HTK888; 1:1667, Cat# n/a, RRID:n/a), αCD8-PerCP-Cy5.5 (clone 53-6 .7, 1:600, Cat# 100734, RRID:AB_2075238),

αCD62L-PE (clone MEL-14; 1:800, Cat# 104407, RRID:AB_313094), αCD62L-Pacific Blue (clone MEL-14; 1:200, Cat# 104423, RRID:AB_493381), αCD44-APC-Cy7 (clone IM7; 1:200), αI-A/I-E-APC-Cy7 (clone M5/114.15.2; 1:200, Cat# 103028, RRID:AB_830785), rat IgG2b κ-APC-Cy7 (clone RTK4530; 1:200, Cat# 400624, RRID:AB_326566), Annexin V-AlexaFluor647 (1:100, Cat# 640911), Annexin V-PE (1:200, Cat# 640908), αCD8-PE (clone 53-6.7, 1:600, Cat# 100708, RRID:AB_312747), αLy-6C/G-APC (clone RB6-8C5, 1:200, Cat# 108412, RRID:AB_313377), αCTLA-4-BV605 (clone UC10-4B9, 1:50, Cat# 106323, RRID:AB_2566467), Armenian hamster IgG-BV605 (clone HTK888; 1:50, Cat# 400943), αTGF-β1-PE (clone TW7-16B4, 1:200, Cat# 141403, RRID:AB_10730610) and IgG1 κ -PE (clone: MOPC-21, Cat# 400113, RRID:AB_326435), αTNFRSF4-BV421 (clone OX-86, 1:50, Cat# 119411, RRID:AB_10962569) and rat IgG1 κ-BV421 (clone RTK2071, 1:50, Cat# 400429, RRID:AB_10900998), αTIGIT-PE-Dazzle (clone: 1G9, 1:100, Cat# 142111, RRID:AB_2687311) and rat IgG1 κ-PE-Dazzle (clone: MOPC-21, 1:100, Cat# 400157, RRID:AB_10897939), αLy-6A/E-APC (clone D7; 1:100, Cat# 108111, RRID:AB_313348) were purchased from BioLegend. αCD8a-BUV395 (clone 53-6.7, 1:600, Cat# 563786, RRID:AB 2732919) and αCD117-BUV395 (clone 2B8, 1:300, Cat# 564011, RRID:AB_2738541) were purchased from BD Biosciences. αCD34-eFluor450 (clone RAM34; 1:100, Cat# 48-0341-82, RRID:AB_2043837), αKi67-PE (clone SolA15, 1:100, Cat# 14-5698-82, RRID:AB_10854564), Rat IgG2a κ-PE-Cy7 (clone eBR2a; 1:100) and αGITR-PE-Cy7 (clone DTA-1, 1:400, Cat# 25-5874-80, RRID:AB_10544396), αCD30-PE (clone: mCD30.1, 1:10, at# 12-0301-81, RRID:AB_465628) and Armenian hamster IgG (clone: eBio299Arm, 1:10, Cat# 12-4888-83, RRID:AB_470074), Viability dye – e450 (1:4000), αMHC I (clone: 28-14-8, 1:100, Cat#: 16-5999-82, RRID: AB_469197) and Rat IgG2b K Isotype Control (clone: eBM2a, 1:100, Cat# 16-4724-82, RRID: AB_470164) and viability dye – e506 (1:1000) were purchased from ThermoFisher. Lineage-positive cells were excluded by MACS-sorting using biotinylated αCD19 (clone 6D5, 1:300, Cat# 115504, RRID:AB_313639), αCD3e (clone 145-

2C11, 1:300, Cat# 100304, RRID:AB_312669), αLy-6G/C (clone RB6-8C5, 1:300, Cat# 108404, RRID:AB_313369) and αTer119 (clone Ter-119; 1:300, Cat# 116203, RRID:AB_313704) from BioLegend, followed by a second staining step with streptavidin-Horizon-V500 (1:1000, Cat# 561419, RRID:AB_10611863) from BD Biosciences after the separation.

Human: αCD34-APC (clone 561, 1:80, Cat# 343607, RRID:AB_2074356) and αCD34-APC-Cy7 (clone 561, 1:100, Cat# 343614, RRID:AB_2571927), αCD45-Pacific-Blue (clone HI30, 1:300, Cat# 304029, RRID:AB_2174123), αCD38-PE-Cy7 (HIT2, 1:50, Cat# 303522, RRID:AB_893314) and αCD90-PerCP-Cy5.5 (clone 5E10, 1:100, Cat# 328117, RRID:AB_961312), αCD3-BV786 (clone: OKT3, 1:100, Cat# 317329, RRID:AB_11219196), aCD4-PE-Cy7 (clone: OKT4, 1:50, Cat# 317414, RRID:AB_571959), αCD25-AF700 (clone: BC96, 1:200, Cat# 302622, RRID:AB_493755), αCD8a-PerCP-Cy5.5 (clone: CD8, 1:100, Cat# 300923, RRID:AB_1575079), αTNFRSF4-PE (clone: Ber-ACT35, 1:30, Cat# 350003, RRID:AB_10641708) and IgG1 κ -PE (clone: MOPC-21, Cat# 400113, RRID:AB_326435) were from BioLegend. αCD127-BUV737 (clone: HIL-7R-M21, 1:50, Cat# 612795, RRID:AB_2870122) was from BD Biosciences.

Lineage-positive cells were excluded by staining using biotinylated αCD2 (clone RPA-2.10, 1:100, 300204, RRID:AB_314028), αCD3 (clone OKT3, 1:100, Cat# 317320, RRID:AB_10916519), αCD14 (clone HCD14, 1:100, at# 325624, RRID:AB_2074052), αCD16 (clone 3G8, 1:100, Cat# 302004, RRID:AB_314204), αCD19 (clone HIB19, 1:100, Cat# 302204, RRID:AB_314234), αCD56 (clone HCD56, 1:100, Cat# 318320, RRID:AB_893390) and αCD235ab (clone HIR2, 1:100, Cat# 306618, RRID:AB_2565773) (BioLegend), followed by a second step using streptavidin-Horizon-V500 (1:1000, BD Pharmingen, Cat# 561419, RRID:AB_10611863).

Flow cytometric analysis on BM and lineage-negative BM cells, blood cells, splenocytes were performed following red blood cell (RBC) lysis. Samples were analyzed on a BD Fortessa and sorting procedures were performed using a BD FACS Aria III (BD Pharmingen). Data were collected using FACSDiva software (BD Pharmingen) analyzed using FlowJo software (Treestar). Effective separation after FACS-sorting was assessed by re-analyzing a fraction of the sorted samples by flow-cytometry analysis (purity after FACS-sorting: 96.2 ± 1.8%).

Patient samples

BM aspirates from untreated, newly diagnosed CML patients at the Department of Hematology and Central Hematology Laboratory, Inselspital, Bern University Hospital and University of Bern, Switzerland, were obtained between 2015-2020. Patient characteristics are listed in Supplementary Table 2. Patient data were collected and managed using REDCap electronic data capture tools hosted at the Department for BioMedical Research (62).

Mice

C57BL/6J (BL/6) mice were purchased from Charles River Laboratories and *Foxp3*$^{DTR/GFP}$ mice were obtained from Jackson Laboratories (33). Major histocompatibility class II$^{-/-}$ (*H2*$^{-/-}$) mice were received from the Swiss Immunological Mouse Repository (63). Perforin$^{-/-}$ (*Prf*$^{-/-}$) mice were kindly provided by P. Krebs (Institute of Pathology, University of Bern, Switzerland)(64). Experiments were performed with age- (6-8 weeks) and sex-matched animals of both genders. Mice were housed under specific pathogen–free conditions in individually ventilated cages with food and water ad libitum and were regularly monitored for pathogens. Mice were assigned to different treatment groups through randomization and all experiments were conducted and analyzed in a non-blinded fashion.

Colony-forming assays

564 Mouse: 5 x 10^3 MACS-purified lin^- cells were plated in semi-solid methylcellulose as
565 previously described (19). GFP^+ colonies were determined after 7 days with an inverted
566 fluorescence microscope.
567 For in vitro co-culture experiments, 10^3 FACS-purified LSCs were incubated with perforin-
568 deficient or -proficient $CD8^+$ T cells from BM of CML mice at a ratio of 1:1 overnight in RPMI
569 supplemented with 10% FCS, 1% Penicillin-Streptomycin, 1% L-Glutamine, SCF (100ng/ml)
570 and TPO (20ng/ml) followed by plating in methylcellulose. Alternatively, LSCs pre-treated
571 with the granzyme B inhibitor I (100µM, Sigma) for 1h at 37°C were co-incubated with $CD8^+$
572 T cells from BM of CML mice at a ratio of 1:1 overnight followed by plating in methylcellulose.
573 In addition, LSCs were co-cultured overnight with $CD8^+$ T cells and Tregs pre-treated for 2h
574 with an Tnfrsf4 antibody (clone OX-86, 30 µg/ml, BioXCell, Cat# BE0031,
575 RRID:AB_1107592) or control IgG1 antibody (Cat# BE0088, RRID:AB_1107775) at a ratio
576 of 1:1:1 in triplicates followed by plating in methylcellulose. For each round of serial colony
577 re-plating, total cells were collected from the methylcellulose, and 10^4 cells were re-plated into
578 methylcellulose without any T cells. Colony numbers were assessed with inverted light
579 microscopy after 7 days for each round of plating (≥30 cells/colony).
580 Human: 10^3 FACS-purified $CD34^+CD38^-$ CML were plated in semi-solid methylcellulose as
581 previously described ((19), Supplementary Table 2). Colonies were determined after 14 days
582 with an inverted light microscope. For co-culture experiments, 10^3 FACS-purified
583 $CD34^+CD38^-$ CML stem/progenitor cells (CML also pre-treated with the granzyme B inhibitor
584 I) were co-incubated with BM $CD8^+$ T cells and/or $CD4^+CD127^{lo}CD25^+$ Tregs at a ratio of
585 1:1:1 followed by plating in methylcellulose. For each round of serial colony re-plating, total
586 cells were collected from the methylcellulose, and 10^4 cells were re-plated into methylcellulose
587 without any T cells. Colony numbers were assessed with inverted light microscopy after 14
588 days for each round of plating (≥30 cells/colony).
589

590 **Leukemia mouse models**

591 Chronic phase CML was induced and monitored as described before (31). Briefly, FACS-
592 purified LSKs from the BM of donor mice were transduced twice on two consecutive days with
593 a BCR-ABL1-GFP retrovirus by spin infection. 3 x 10^4 cells were injected intravenously into
594 the tail vein of non-irradiated syngeneic recipients.

595 Blast crisis CML was induced as previously described (65). FACS-purified LSKs were
596 simultaneously transduced with BCR-ABL1-CFP and NUP98-HOX-GFP retrovirus in a
597 RetroNectin pre-coated plate on two consecutive days. After two transduction rounds, NUP98-
598 HOX-GFP/ BCR-ABL1-CFP double-positive cells were FACS-purified and injected into
599 sublethally irradiated recipients (4.5 Gy) to expand the leukemic cells. 5 x 10^3 NUP98-HOX-
600 GFP/ BCR-ABL1-CFP double-positive cells from primary recipient mice were injected
601 intravenously into the tail vein of non-irradiated syngeneic recipients.

602 For Treg depletion, DT (15ng/g, Sigma) was administered intraperitoneally (i.p.) at different
603 days indicated in the figure legends. Sterile PBS (Sigma) was used as a control treatment. To
604 deplete CD8α,β T cells, mice were treated with 75μg murine αCD8α mAb (clone: 53-6.7,
605 BioXCell, Cat# BE0004-1, RRID:AB_1107671) i.p. at different days indicated in the figure
606 legends. To compare LSC activity in vivo, 5 x 10^6 WBM cells from primary CML mice were
607 injected intravenously into lethally irradiated (6.5 Gy twice with 4 hours interval) secondary
608 recipient mice.

609 For Tnfrsf4 antibody treatment experiments, Tnfrsf4 antibody (200μg/mouse, clone, OX-86,
610 BioXCell, Cat# BE0031, RRID:AB_1107592) was administered intraperitoneally (i.p.). for six
611 times every second day, starting at day 12. Rat IgG1, κ (BioXCell, Cat# BE0088,
612 RRID:AB_1107775) was used as a control treatment.

613

614 **LSC analysis**

The LSC numbers in chronic phase and blast-crisis CML mice were analyzed phenotypically by FACS analysis as previously described(18, 19). Briefly, LSC subpopulations in BCR-ABL1-GFP$^+$ lin$^-$ BM cells were defined as follows: L-HPC-1 (Sca-1$^+$c-kit^{high}CD48$^+$CD150$^-$), L-HPC-2 (Sca-1$^+$c-kit^{high}CD48$^+$CD150$^+$), L-MPPs (Sca-1$^+$c-kit^{high}CD48$^-$CD150$^-$) and LT-LSCs (Sca-1$^+$c-kit^{high}CD48$^-$CD150$^+$). For blast-crisis CML, the disease-initiating cells were defined as NUP98-HOX-GFP$^+$BCR-ABL1-CFP$^+$lin$^-$Sca-1$^+$c-kit^{high}CD135$^+$CD150$^-$ (66).

Ki67 staining

Ki67 staining was performed with Foxp3/Transcription Factor Staining Buffer Set (ThermoFisher) according to manufacturer's protocol. After surface marker staining, cells were incubated in fixation/permeabilization working solution for up to 18h at 4°C, followed by washing with permeabilization buffer and intracellular staining with Ki-67 PE antibody for 30min at 4°C.

High-throughput transcriptome analysis using next generation RNA sequencing (RNA-Seq)

Total RNA was extracted from Tregs derived from the BM of naïve and CML-bearing *Foxp3*$^{DTR/GFP}$ mice (n=3/group) using the RNeasy Micro Kit (cat. 74004, Qiagen). Total RNA quality was determined by a Bioanalyzer using the RNA 6000 Nano Chip (Agilent Technologies) and quantified by fluorometry using the Quantifluor RNA System Kit (cat. E3310, Promega) on a Quantus Fluorometer Instrument (Promega).

Library preparation was performed from total RNA using the SMART-Seq v4 Ultra Low Input RNA Kit for Sequencing (Takara Bio). Libraries were quality-checked on the Fragment Analyzer using the High Sensitivity NGS Fragment Analysis Kit (Agilent). Samples were pooled to equal molarity and the pool was quantified by fluorometry, in order to be loaded at a final concentration of 2pM on the NextSeq 500 instrument (Illumina). Samples were sequenced

SR76 using the NextSeq 500 High Output Kit 75-cycles (Illumina) and primary data analysis was performed using the Illumina RTA version 2.4.11 and bcl2fastq v2.20.0.422.

RNA-Seq data analysis

The RNA-Seq data was assembled by SeqMan NGen software v.15 and analyzed using ArrayStar software v.15 (DNASTAR, USA). The software allows statistical analyses of differential gene expression using EdgeR or DESeq2. For our analysis we used DEseq2. The level of gene expression was assessed after normalization and log2 transformation. The data set was analyzed by two-way ANOVA. Genes with significant difference in their expression at FDR-P<0.05 and fold differences ≥1.5 were selected. Data were clustered using standard Euclidean's method based on the average linkage and heatmaps were generated according to the standard normal distribution of the values.

Gene ontology analysis

Gene ontology (GO) enrichment was assessed using Partek® Genomics Suite™ software, v.7 (Partek). The list of differently expressed genes was grouped into functional hierarchies. Enrichment scores were calculated using a chi-square test comparing the proportion of the gene list in a group to the proportion of the background genes. A value of 3 or higher corresponded to a significant over-expression (P<0.05).

qRT-PCR

For qRT-PCR, total RNA was extracted using the Quick-RNA MiniPrep kit (Zymo Research). Complementary DNA synthesis was performed using $2.5x10^{-4}$ units/µl hexanucleotide mix (Roche), 0.4mM deoxynucleotide mix (Sigma), 1.25 units/µl RNAsin and 4 units/µl reverse transcriptase (Promega). Gene expression analysis was accomplished for murine *Gzma* and *Gzmb* using self-designed primers and SYBR green reaction (Roche; *Gzma,* FV:

CACTGTAACGTGGGAAAGAG, RV: GTGAAGGATAGCCACATTTCTG; *Gzmb,* FV: CTGCTAAAGCTGAAGAGTAAGG, RV: GCTCAACCTCTTGTAGCGT). Samples were measured in duplicates or triplicates including non-template controls using a QuantStudio 3 Real-Time PCR system (Applied Biosystems). Relative quantification of gene expression was normalized against a reference gene (*Gapdh or* ACTB) and calculated as an exponent of 2 ($2^{\Delta Ct}$).

Immunhistochemistry

Human: To study the distribution of $FOXP3^+$ Tregs and their spatial proximity to $CD34^+$ and $CD8^+$ cells, FFPE tissues from 10 CML and 4 control BM core biopsies were analyzed. Sections were cut to 2 um thickness and IHC double stainings of full slides were performed for both FOXP3/CD8 and FOXP3/CD34 (anti-human FOXP3, eBioscience, 1:200, Cat# 14-4777-80, RRID:AB_467555; anti-human CD8, 1:100, Cat# M7103, RRID:AB_2075537; anti-human CD34, 1:50, Cell Marque, Cat# 134M-16, RRID:AB_1159227) using a Leica BOND RX automated immunostainer (Leica Biosystems). A counting field of $1{,}2mm^2$ was randomly selected and $FOXP3^+$ Tregs were counted at 20x magnification in CML and control BM biopsies (HD). Close proximity between $FOXP3^+$ Tregs and $CD8^+$ or $CD34^+$ LSPCs was defined as a distance of less than or equal to two cell nuclei. Since $FOXP3^+$ Tregs were observed at a low frequency in control BM biopsies and to enable a sufficient comparison between control BM and CML biopsies, control BM biopsies with less than 5 $FOXP3^+$ Tregs (counted in 1,2mm2) were additionally screened longitudinally for additional Tregs that could be included into the final analysis.

Mouse: The distribution of $FOXP3^+$ Tregs and their spatial proximity to $CD8^+$ cells was analyzed using FFPE tissues from 8 CML and 9 control murine BM core biopsies. Sections were cut to 2.5 μm thickness and IHC double stainings of full slides were performed for FOXP3/CD8 (rat anti-mouse FOXP3, clone FJK-16s, eBioscience, 1:00, Cat# 14-5773-80,

693 RRID:AB_467576; rat anti-mouse CD8, clone 4SM15, 1:100, eBioscience Cat# 14-0808-80,
694 RRID:AB_2572861) using a Ventana Discovery ULTRA automated immunostainer (Roche
695 Diagnostics). A counting field of 1,2mm^2 was randomly selected and FOXP3$^+$ Tregs were
696 counted at 20x magnification in CML and control BM biopsies. Close proximity between
697 FOXP3$^+$ Tregs and CD8$^+$ cells was defined as a distance of less than or equal to two cell nuclei.
698 To illustrate the distribution pattern of FOXP3$^+$ cells in human and murine control and CML
699 BM core biopsies, whole slides were analyzed using QuPath (software version 0.1.2)(67).
700
701 **Statistics**
702 Statistical analysis was performed using GraphPad Prism 7.04 (GraphPad Software). Statistical
703 tests applied to determine significance for each experiment are detailed in the corresponding
704 figure legend. Data are represented as mean ± SEM and assumed to distribute normally. For
705 Treg depletion experiments, leukemia load was determined in the blood when disease was
706 established, and mice were randomized using GraphPad software random number generator to
707 the different treatment groups based on disease burden. Data were analyzed using Student's t-
708 test (two-sided), one-way ANOVA followed by Tukey's or Dunnett's post-test (two-sided) and
709 two-way ANOVA followed by Sidak's post-test (two-sided). Significant differences in Kaplan-
710 Meier survival curves were determined using the log-rank test. Human data from the microarray
711 dataset were checked with column statistics for normal distribution and analyzed with Student's
712 t-test (two-sided). Correlations were determined using Spearman correlations (two-sided). All
713 *P*-values were considered as significant when $P<0.05$. All experiments were at least performed
714 twice in independent experiments.
715
716 **Study approval**

Animal experiments were approved by the local experimental animal committee of the Canton of Bern and performed according to Swiss laws for animal protection (KEK 75/17, 78/17, BE56/20 and BE59/20).

Analysis of BM samples was approved by the local ethical committee of the Canton of Bern, Switzerland (KEK 122/14 and 2019-01627). Written informed consent was collected from all patients who donated BM.

Materials Availability

All unique reagent generated in this study are available from the corresponding author without restriction.

Data and Code Availability

All RNA-seq data compiled for this study are made publicly available on the Gene Expression Omnibus (GEO) website (http://www.ncbi.nlm.nih.gov/geo/) under the accession number GSE174190. This study does not include the development of new code.

Author contributions: M.H. designed and performed experiments, analyzed and interpreted data and contributed to the preparation and writing of the manuscript. V.R., designed and performed experiments, analyzed and interpreted data. C.S., S.F., R.R and N.S. designed and performed experiments and analyzed data. G.M.B. collected and contributed CML patient samples and interpreted data. A.F.O. interpreted data, designed experiments and revised the manuscript. C.R. designed and supervised the study, interpreted data and wrote the manuscript. All authors revised the manuscript and approved its final version.

Acknowledgements: We thank the staff of the FACSlab (Department for BioMedical Research (DBMR), University of Bern, Switzerland) and the TRU team (Institute of Pathology University of Bern, Switzerland) for providing excellent technical assistance. We thank the EPFL Histology Core Facility for performing the double IHC Foxp3/Cd8 on mouse tissue sections. We also thank Ursina Lüthi, Tanja Chiorazzo and Michalea Römmele for their outstanding technical support and work for this project. This work was supported by grants from the Swiss National Science Foundation (310030_179394), the Alfred und Anneliese Sutter-Stöttner Stiftung and the Stiftung für klinisch-experimentelle Tumorforschung (all to C.R.).

References

1. Cortes JE et al. Ponatinib efficacy and safety in Philadelphia chromosome–positive leukemia: final 5-year results of the phase 2 PACE trial. *Blood* 2018;132(4):393–404.

2. Larson RA et al. Nilotinib vs imatinib in patients with newly diagnosed Philadelphia chromosome-positive chronic myeloid leukemia in chronic phase: ENESTnd 3-year follow-up. *Leukemia* 2012;26(10):2197–2203.

3. Kantarjian HM et al. Nilotinib versus imatinib for the treatment of patients with newly diagnosed chronic phase, Philadelphia chromosome-positive, chronic myeloid leukaemia: 24-month minimum follow-up of the phase 3 randomised ENESTnd trial. *Lancet Oncol.* 2011;12(9):841–851.

4. Laneuville P. Stopping second-generation TKIs in CML. *Blood* 2017;129(7):805–806.

5. Holyoake TL, Vetrie D. The chronic myeloid leukemia stem cell: stemming the tide of persistence. *Blood* 2017;129(12):1595–1606.

6. Weiden PL et al. Antileukemic Effect of Graft-versus-Host Disease in Human Recipients of Allogeneic-Marrow Grafts. *N. Engl. J. Med.* 1979;300(19):1068–1073.

7. Kolb HJ et al. Graft-versus-leukemia effect of donor lymphocyte transfusions in marrow grafted patients.. *Blood* 1995;86(5):2041–50.

8. Gale RP. Identical-Twin Bone Marrow Transplants for Leukemia. *Ann. Intern. Med.* 1994;120(8):646.

9. Sehn LH et al. Comparative Outcomes of T-Cell–Depleted and Non–T-Cell–Depleted Allogeneic Bone Marrow Transplantation for Chronic Myelogenous Leukemia: Impact of Donor Lymphocyte Infusion. *J. Clin. Oncol.* 1999;17(2):561–561.

10. Horowitz MM et al. Graft-versus-leukemia reactions after bone marrow transplantation.. *Blood* 1990;75(3):555–62.

11. Ross DM et al. Safety and efficacy of imatinib cessation for CML patients with stable undetectable minimal residual disease: results from the TWISTER study. *Blood* 2013;122(4):515–522.

12. Houshmand M et al. Chronic myeloid leukemia stem cells. *Leukemia* 2019;33(7):1543–1556.

13. Schumacher TN, Schreiber RD. Neoantigens in cancer immunotherapy. *Science (80-.).* 2015;348(6230):69–74.

14. Rezvani K et al. Functional leukemia-associated antigen-specific memory CD8+ T cells exist in healthy individuals and in patients with chronic myelogenous leukemia before and after stem cell transplantation. *Blood* 2003;102(8):2892–2900.

15. Yotnda P et al. Cytotoxic T cell response against the chimeric p210 BCR-ABL protein in patients with chronic myelogenous leukemia.. *J. Clin. Invest.* 1998;101(10):2290–2296.

16. Clark RE et al. Direct evidence that leukemic cells present HLA-associated immunogenic peptides derived from the BCR-ABL b3a2 fusion protein. *Blood* 2001;98(10):2887–2893.

17. Bilich T et al. The HLA ligandome landscape of chronic myeloid leukemia delineates novel T-cell epitopes for immunotherapy. *Blood* 2019;133(6):550–565.

18. Riether C, Gschwend T, Huguenin AL, Schürch CM, Ochsenbein AF. Blocking

795 programmed cell death 1 in combination with adoptive cytotoxic T-cell transfer eradicates
796 chronic myelogenous leukemia stem cells. *Leukemia* 2015;29(8):1781–1785.
797 19. Schurch C, Riether C, Amrein MA, Ochsenbein AF. Cytotoxic T cells induce proliferation
798 of chronic myeloid leukemia stem cells by secreting interferon-gamma. *J. Exp. Med.*
799 2013;210(3):605–621.
800 20. Tarafdar A et al. CML cells actively evade host immune surveillance through cytokine-
801 mediated downregulation of MHC-II expression. *Blood* 2017;129(2):199–208.
802 21. Schurch C, Riether C, Matter MS, Tzankov A, Ochsenbein AF. CD27 signaling on
803 chronic myelogenous leukemia stem cells activates Wnt target genes and promotes disease
804 progression. *J. Clin. Invest.* 2012;122(2):624–638.
805 22. Fujisaki J et al. In vivo imaging of Treg cells providing immune privilege to the
806 haematopoietic stem-cell niche. *Nature* 2011;474(7350):216–219.
807 23. Brück O et al. Immune cell contexture in the bone marrow tumor microenvironment
808 impacts therapy response in CML. *Leukemia* 2018;32(7):1643–1656.
809 24. Hus I et al. Evaluation of monocyte-derived dendritic cells, T regulatory and Th17 cells in
810 chronic myeloid leukemia patients treated with tyrosine kinase inhibitors. *Folia Histochem.*
811 *Cytobiol.* 2011;49(1):153–160.
812 25. Bachy E, Bernaud J, Roy P, Rigal D, Nicolini FE. Quantitative and functional analyses of
813 CD4+CD25+FoxP3+ regulatory T cells in chronic phase chronic myeloid leukaemia patients
814 at diagnosis and on imatinib mesylate. *Br. J. Haematol.* 2011;153(1):139–143.
815 26. Zahran AM, Badrawy H, Ibrahim A. Prognostic value of regulatory T cells in newly
816 diagnosed chronic myeloid leukemia patients. *Int. J. Clin. Oncol.* 2014;19(4):753–760.
817 27. Rojas JM et al. Naturally occurring CD4+ CD25+ FOXP3+ T-regulatory cells are
818 increased in chronic myeloid leukemia patients not in complete cytogenetic remission and can
819 be immunosuppressive. *Exp. Hematol.* 2010;38(12):1209–1218.
820 28. Najima Y et al. Regulatory T cell inhibition by dasatinib is associated with natural killer

821 cell differentiation and a favorable molecular response—The final results of the D-first study.
822 *Leuk. Res.* 2018;66:66–72.
823 29. Hughes A, Yong ASM. Immune Effector Recovery in Chronic Myeloid Leukemia and
824 Treatment-Free Remission.. *Front. Immunol.* 2017;8:469.
825 30. Irani YD et al. Successful treatment-free remission in chronic myeloid leukaemia and its
826 association with reduced immune suppressors and increased natural killer cells. *Br. J.*
827 *Haematol.* 2020;191(3):433–441.
828 31. Riether C et al. Metoclopramide treatment blocks CD93-signaling-mediated self-renewal
829 of chronic myeloid leukemia stem cells. *Cell Rep.* 2021;34(4):108663.
830 32. Singh K, Hjort M, Thorvaldson L, Sandler S. Concomitant analysis of Helios and
831 Neuropilin-1 as a marker to detect thymic derived regulatory T cells in naïve mice. *Sci. Rep.*
832 2015;5(1):7767.
833 33. Kim JM, Rasmussen JP, Rudensky AY. Regulatory T cells prevent catastrophic
834 autoimmunity throughout the lifespan of mice. *Nat. Immunol.* 2007;8(2):191–197.
835 34. Martinez-Lostao L, Anel A, Pardo J. How Do Cytotoxic Lymphocytes Kill Cancer Cells?.
836 *Clin. Cancer Res.* 2015;21(22):5047–5056.
837 35. Zhang B et al. Inhibition of interleukin-1 signaling enhances elimination of tyrosine
838 kinase inhibitor–treated CML stem cells. *Blood* 2016;128(23):2671–2682.
839 36. Li MO, Rudensky AY. T cell receptor signalling in the control of regulatory T cell
840 differentiation and function. *Nat. Rev. Immunol.* 2016;16(4):220–233.
841 37. Vahl JC et al. Continuous T Cell Receptor Signals Maintain a Functional Regulatory T
842 Cell Pool. *Immunity* 2014;41(5):722–736.
843 38. Levine AG, Arvey A, Jin W, Rudensky AY. Continuous requirement for the TCR in
844 regulatory T cell function. *Nat. Immunol.* 2014;15(11):1070–1078.
845 39. Rebel VI et al. Essential Role for the P55 Tumor Necrosis Factor Receptor in Regulating
846 Hematopoiesis at a Stem Cell Level. *J. Exp. Med.* 1999;190(10):1493–1504.

40. Lee S-W et al. Identification of regulatory functions for 4-1BB and 4-1BBL in myelopoiesis and the development of dendritic cells. *Nat. Immunol.* 2008;9(8):917–926.

41. Jiang D, Schwarz H. Regulation of Granulocyte and Macrophage Populations of Murine Bone Marrow Cells by G-CSF and CD137 Protein. *PLoS One* 2010;5(12):e15565.

42. Piconese S, Valzasina B, Colombo MP. OX40 triggering blocks suppression by regulatory T cells and facilitates tumor rejection. *J. Exp. Med.* 2008;205(4):825–839.

43. Valzasina B et al. Triggering of OX40 (CD134) on CD4+CD25+ T cells blocks their inhibitory activity: a novel regulatory role for OX40 and its comparison with GITR. *Blood* 2005;105(7):2845–2851.

44. Vu MD et al. OX40 costimulation turns off Foxp3+ Tregs. *Blood* 2007;110(7):2501–2510.

45. Bulliard Y et al. OX40 engagement depletes intratumoral Tregs via activating FcγRs, leading to antitumor efficacy. *Immunol. Cell Biol.* 2014;92(6):475–480.

46. Riether C, Schurch CM, Ochsenbein AF. Regulation of hematopoietic and leukemic stem cells by the immune system. *Cell Death Differ.* 2015;22(2):187–198.

47. Gallipoli P et al. Autocrine TNF-α production supports CML stem and progenitor cell survival and enhances their proliferation. *Blood* 2013;122(19):3335–3339.

48. Kagoya Y et al. Positive feedback between NF-κB and TNF-α promotes leukemia-initiating cell capacity. *J. Clin. Invest.* 2014;124(2):528–542.

49. Camacho V et al. Bone marrow Tregs mediate stromal cell function and support hematopoiesis via IL-10.. *JCI insight* 2020;5(22). doi:10.1172/jci.insight.135681

50. Togashi Y, Shitara K, Nishikawa H. Regulatory T cells in cancer immunosuppression — implications for anticancer therapy. *Nat. Rev. Clin. Oncol.* 2019;16(6):356–371.

51. Yasukawa M et al. HLA class II-restricted antigen presentation of endogenous bcr-abl fusion protein by chronic myelogenous leukemia-derived dendritic cells to CD4(+) T lymphocytes.. *Blood* 2001;98(5):1498–505.

873 52. Mannering SI, McKenzie JL, Fearnley DB, Hart DN. HLA-DR1-restricted bcr-abl (b3a2)-
874 specific CD4+ T lymphocytes respond to dendritic cells pulsed with b3a2 peptide and
875 antigen-presenting cells exposed to b3a2 containing cell lysates.. *Blood* 1997;90(1):290–7.
876 53. Bosch GJ, Joosten AM, Kessler JH, Melief CJ, Leeksma OC. Recognition of BCR-ABL
877 positive leukemic blasts by human CD4+ T cells elicited by primary in vitro immunization
878 with a BCR-ABL breakpoint peptide.. *Blood* 1996;88(9):3522–7.
879 54. Schmidt H-H et al. HLA Class II tetramers reveal tissue-specific regulatory T cells that
880 suppress T-cell responses in breast carcinoma patients. *Oncoimmunology* 2013;2(6):e24962.
881 55. François V et al. The CD4 + T-Cell Response of Melanoma Patients to a MAGE-A3
882 Peptide Vaccine Involves Potential Regulatory T Cells. *Cancer Res.* 2009;69(10):4335–4345.
883 56. Wang HY et al. Tumor-Specific Human CD4+ Regulatory T Cells and Their Ligands.
884 *Immunity* 2004;20(1):107–118.
885 57. Ahmadzadeh M et al. Tumor-infiltrating human CD4 + regulatory T cells display a
886 distinct TCR repertoire and exhibit tumor and neoantigen reactivity. *Sci. Immunol.*
887 2019;4(31):eaao4310.
888 58. Manlove LS et al. Adaptive Immunity to Leukemia Is Inhibited by Cross-Reactive
889 Induced Regulatory T Cells. *J. Immunol.* 2015;195(8):4028–4037.
890 59. Alexandrov LB et al. Signatures of mutational processes in human cancer. *Nature*
891 2013;500(7463):415–421.
892 60. Butt NM et al. Circulating bcr-abl-specific CD8+ T cells in chronic myeloid leukemia
893 patients and healthy subjects.. *Haematologica* 2005;90(10):1315–23.
894 61. Hirata Y et al. CD150high Bone Marrow Tregs Maintain Hematopoietic Stem Cell
895 Quiescence and Immune Privilege via Adenosine. *Cell Stem Cell* 2018;22(3):445-453.e5.
896 62. Harris PA et al. Research electronic data capture (REDCap)--a metadata-driven
897 methodology and workflow process for providing translational research informatics support.
898 *J. Biomed. Inform.* 2009;42(2):377–381.

63. Madsen L et al. Mice lacking all conventional MHC class II genes. *Proc. Natl. Acad. Sci.* 1999;96(18):10338–10343.

64. Kägi D et al. Cytotoxicity mediated by T cells and natural killer cells is greatly impaired in perforin-deficient mice. *Nature* 1994;369(6475):31–37.

65. Mumprecht S, Schürch C, Schwaller J, Solenthaler M, Ochsenbein AF. Programmed death 1 signaling on chronic myeloid leukemia–specific T cells results in T-cell exhaustion and disease progression. *Blood* 2009;114(8):1528–1536.

66. Neering SJ et al. Leukemia stem cells in a genetically defined murine model of blast-crisis CML. *Blood* 2007;110(7):2578–2585.

67. Bankhead P et al. QuPath: Open source software for digital pathology image analysis. *Sci. Rep.* 2017;7(1):16878.

Figures and Figure legends:

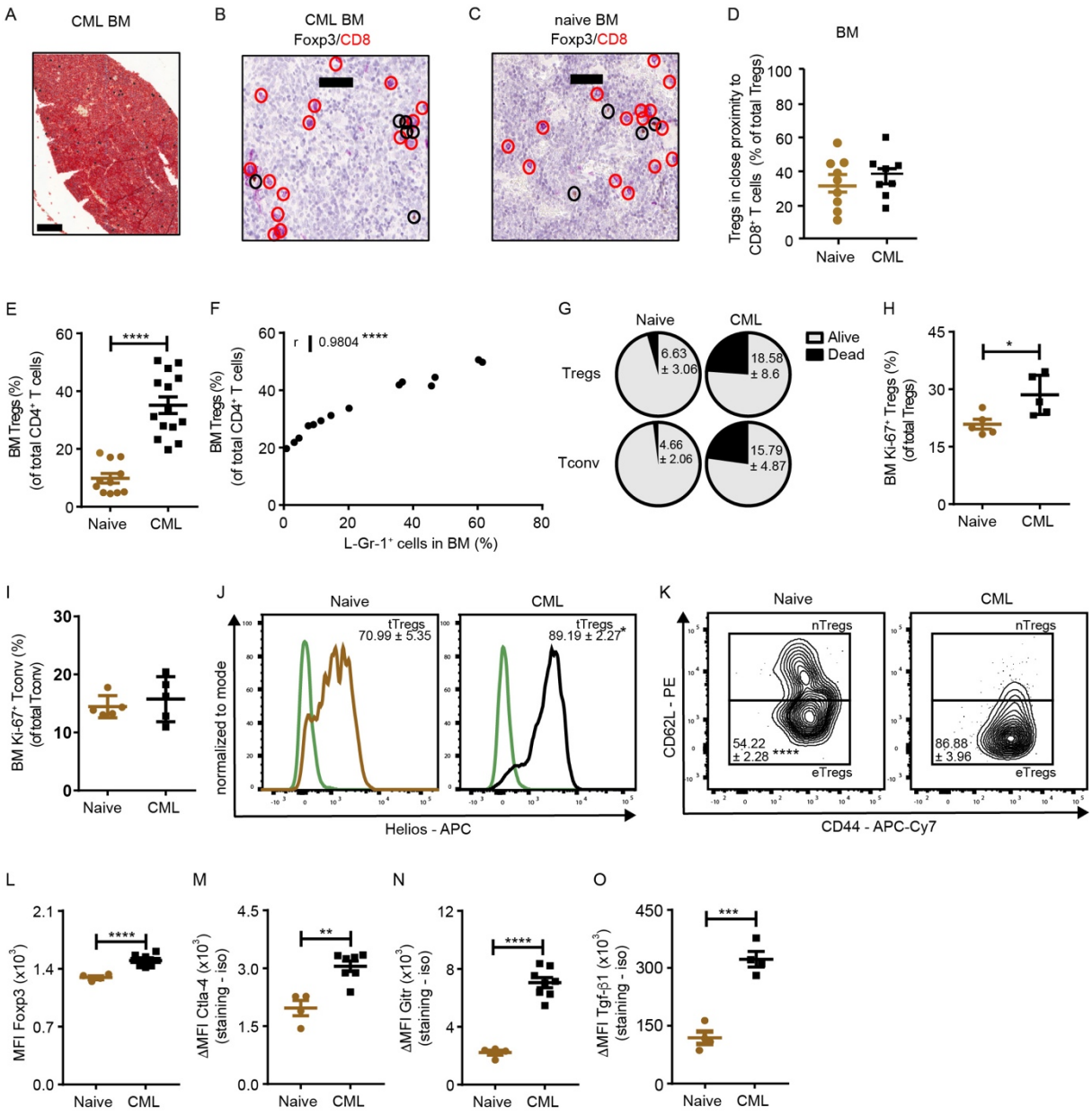

Figure 1: Thymic-derived effector Tregs accumulate in the BM of CML mice. (A) Distribution of Foxp3$^+$ Tregs in CML BM (day 14, scale bar 200µm, n=8 mice). **(B, C)** Distribution of Foxp3$^+$ Tregs in the BM of **(B)** CML mice (n=8) and **(C)** naïve mice (n=9) in respect to CTLs (scale bar 50µm; Foxp3: brown; CD8: red). Black circles: Foxp3$^+$ cells; Red circles: CTLs close to Tregs. **(D)** Frequency of Tregs located close to CTLs in the BM naïve and CML mice (naive: n=9 mice; CML: n=8 mice). Close proximity was defined as a distance of $\leq$ two cell nuclei; t-test. (**E**) Frequency of BM Tregs within total CD4$^+$ T cell population in naive (n=11) and CML (n=14) *Foxp3*^{DTR} mice; t-test. (**F**) Correlation between frequencies of Tregs (within total CD4$^+$ T cells) and L-Gr-1$^+$ cells in the BM of *Foxp3*^{DTR} CML mice (n=14);

Pearson correlation (two-sided). **(G)** Viability of Tregs and Tconv from naive and *Foxp3*^{DTR} CML mice (naive: n=5 mice; CML: n=9 mice); t-test **(H, I)** Proliferation of **(H)** BM Tregs and **(I)** Tconv from naive and *Foxp3*^{DTR} CML mice (naive: n=5 mice; CML: n=5 mice). **(J)** Representative histogram for Helios^{+} thymic-derived Tregs (tTregs) and Helios^{-} peripheral-induced Tregs (pTregs) in the BM of naïve (n=11) and CML *Foxp3*^{DTR} mice (n=8). Pre-gated on CD4^{+} Foxp3-GFP^{+} Tregs. Staining: beige (naïve) and black (CML), isotype: green; t-test. **(K)** Representative Zebra-Plot for naive/resting Tregs (nTregs) and effector Tregs (eTregs) in the BM of naïve (n=5) and CML *Foxp3*^{DTR} mice (n=5); t-test. **(L)** MFI Foxp3 expression (GFP^{+}), ΔMFI of **(M)** Ctla-4, **(N)** Gitr and **(O)** Tgf-β1 on CD4^{+} Foxp3-GFP^{+} Tregs in the BM naïve (n=4) and CML *Foxp3*^{DTR} mice (n=4-8); t-test. ΔMFI=staining-isotype. Data are displayed as mean±SEM. * P<0.05, ** P<0.01, *** P<0.001 and **** P<0.0001.

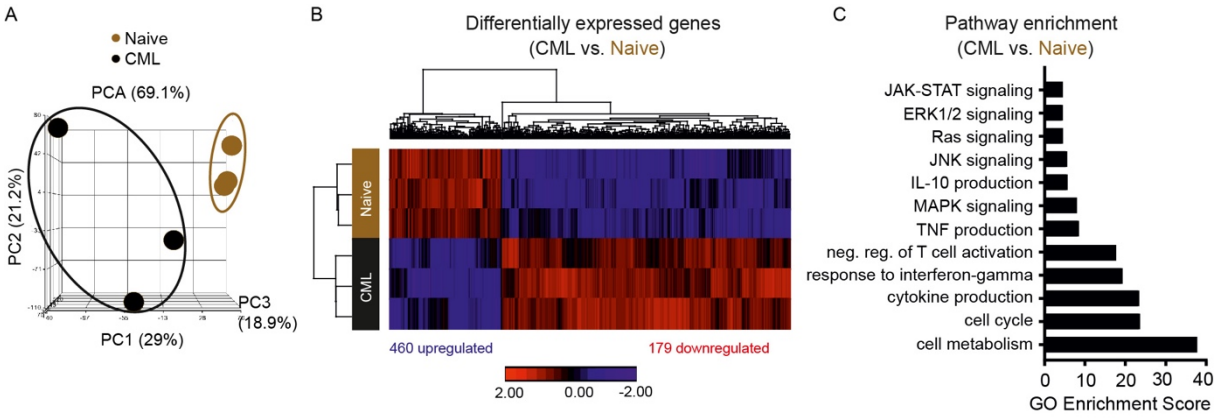

Figure 2: NGS RNA sequencing analysis of Tregs derived from the BM of naïve and CML mice. (A) Principal component analysis (PCA), **(B)** Heatmap of differentially expressed genes and **(C)** Gene ontology (GO) analysis of Tregs derived from BM CML and naïve *Foxp3*^{DTR} mice (n=3 mice/group) upon transcriptomic analysis.

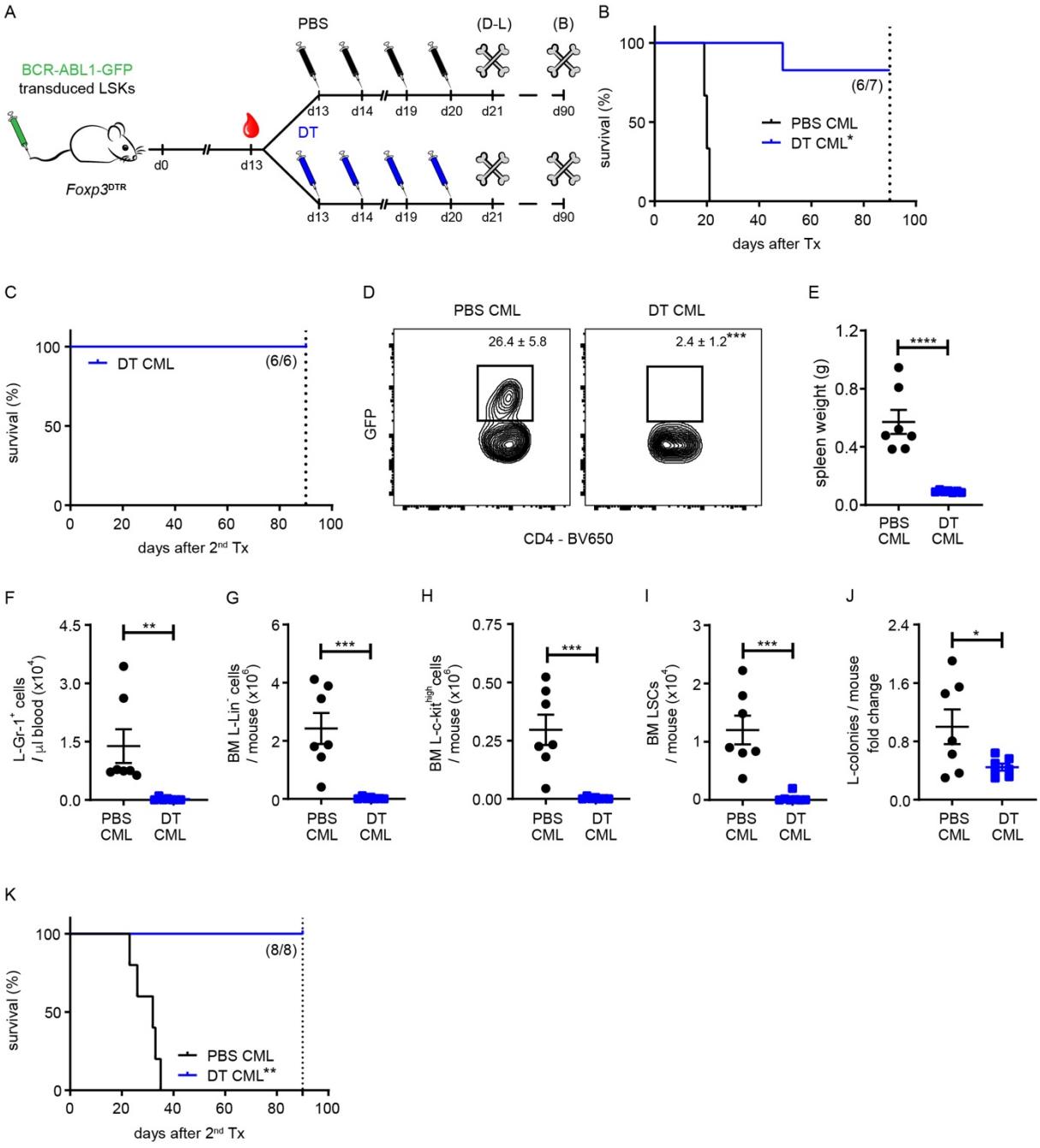

Figure 3: Treg depletion reduces CML LSC numbers in vivo. (**A**) Experimental setup. BCR-ABL1-GFP-transduced LSKs were injected intravenously into non-irradiated *Foxp3*^{DTR} recipients. After establishment of the disease (day 13), mice were randomized to DT or PBS treatment (d13, 14, 19 and 20, i.p.). **(B)** Kaplan-Meier survival curves of PBS- and DT-treated CML mice (PBS: n=7, DT: n=7); log-rank test. (**C**) Kaplan-Meier survival curve of secondary CML mice. BM cells of surviving primary CML mice were injected i.v. into lethally irradiated secondary BL/6 recipients and survival was monitored (n=6 surviving DT CML mice). (**D**) BM

CD4$^+$Foxp3-GFP$^+$ Tregs, **(E)** Spleen weight, (**F**) L-Gr-1$^+$ cells, and absolute numbers of **(G)** L-lin$^-$ cells, **(H)** L-c-kit^{high}, **(I)** LSCs in BM and (**J**) Colony formation capacity per mouse was determined 21 days after CML induction (PBS: n=7; DT: n=8); t-tests. (**K**) BM cells of primary CML mice (d21) were injected i.v. into lethally irradiated secondary BL/6 recipients and survival was monitored (PBS: n=7; DT: n=8); log-rank test. Data are displayed as mean±SEM. * P<0.05, ** P<0.01, *** P<0.001 and **** P<0.0001. Dotted lines represent the time point of the experiment termination at day 90.

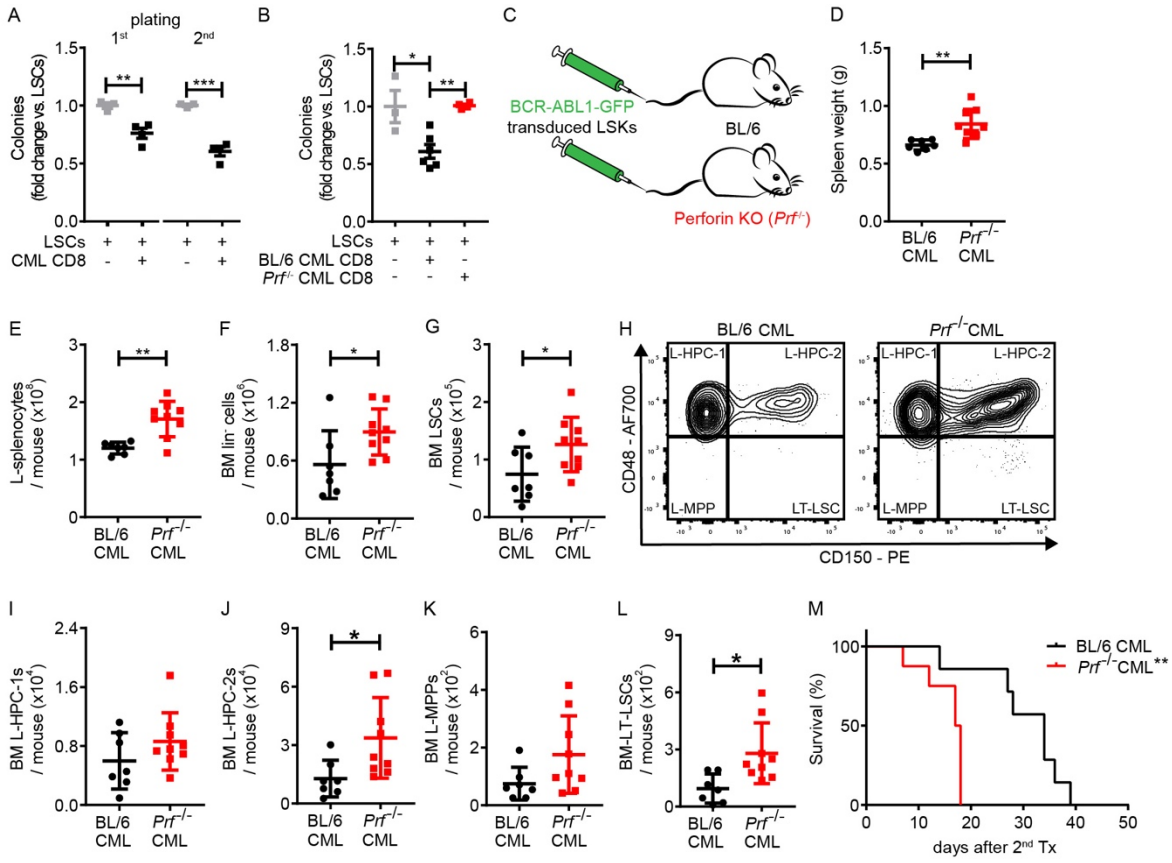

Figure 4: CD8$^+$ CTLs from the BM of CML mice eradicate LSCs by perforin-mediated killing in vitro and in vivo. (A) BL/6 LSCs were cultured in the presence and absence of BM CD8$^+$ CTLs from CML-bearing BL/6 overnight at a ratio of 1:1 in triplicates followed by plating in methylcellulose. Colonies were enumerated 7 days later. For secondary platings, cells isolated from primary colony assays were re-plated in methylcellulose in the absence of T cells; t-est (Groups: LSCs: n=3 mice, LSCs + CML CD8: n=4). **(B)** BL/6 LSCs were cultured

overnight in the presence and absence of $CD8^+$ CTLs derived from the BM of perforin-proficient and –deficient CML mice at a ratio of 1:1 in triplicates followed by plating in methylcellulose. Colonies were enumerated 7 days later; One-way ANOVA followed by Tukey's multiple comparison (Groups: LSCs: n=3 mice, LSCs + BL/6 CML CD8: n=6, LSCs + *Prf*$^{-/-}$ CML CD8: n=4). **(C to L)** BCR-ABL1-GFP-transduced LSKs were injected intravenously into non-irradiated BL/6 (n=7) and *Prf*$^{-/-}$ (n=8) recipient mice. **(D)** Spleen weight; t-test (BL/6 CML: n=7 mice, *Prf*$^{-/-}$ CML: n=8 mice), **(E)** absolute numbers of L-splenocytes, **(F)** of L-lin^- and **(G)** LSCs in the BM of CML mice; t-test (BL/6 CML: n=7 mice, *Prf*$^{-/-}$ CML: n=8 mice) 15 days after CML induction. **(H)** Gating strategy to define LSC subpopulations; cells are pre-gated on lin^- $GFP^+Sca\text{-}1^+c\text{-}kit^+$ cells. Representative images from one out of n=7 (BL/6) and one out of n=8 *Prf*$^{-/-}$ CML mice are shown. **(I to L)** Absolute numbers of LSC subpopulations; t-tests (BL/6 CML: n=7 mice, *Prf*$^{-/-}$ CML: n=8 mice). (**M**) BM cells from primary BL/6 (n=7) and *Prf*$^{-/-}$ (n=8) CML mice were injected intravenously into lethally irradiated secondary BL/6 recipients and survival was monitored; log-rank test. Data are displayed as mean ± SEM. * $P<0.05$, ** $P<0.01$ and *** $P<0.001$.

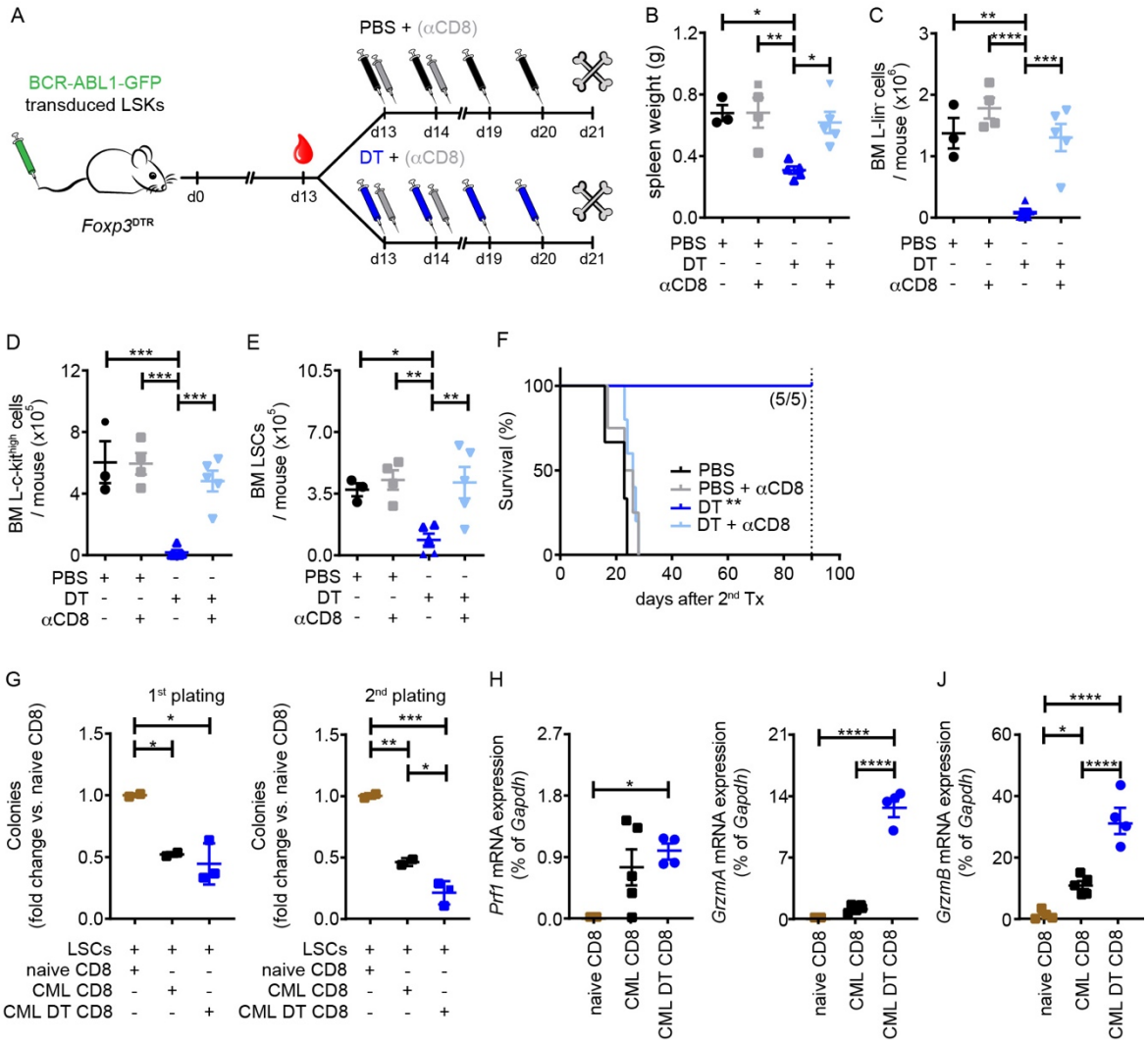

Figure 5: BM Tregs in CML protect LSCs from CD8$^+$ T cell-mediated eradication in vivo. (**A**) Experimental setup. BCR-ABL1-GFP-transduced LSKs were injected intravenously into non-irradiated *Foxp3*^{DTR} recipients. At day 13, mice were randomized to PBS/DT and αCD8 mAb treatment (DT: i.p. at days 13, 14, 19 and 20; αCD8 mAb at days 13 and 15 i.p). **(B)** Spleen weight, **(C)** Absolute numbers of L-lin$^-$ cells, **(D)** L-c-kit^{high} cells and **(E)** LSCs in the BM of CML mice of all treatment groups 21 days after CML induction; One-way ANOVAs followed by Tukey's multiple comparison test. (Groups: PBS: n=3 mice, PBS + αCD8: n=4 mice, DT: n=5 mice and DT + αCD8: n=5 mice). **(F)** BM cells of primary CML mice (d21) were injected i.v. into lethally irradiated secondary BL/6 recipients and survival was monitored; log-rank test. (Groups: PBS: n=3 mice, PBS + αCD8: n=4 mice, DT: n=5 mice and DT + αCD8: n=5 mice). **(G)** LSCs were pre-incubated with CD8$^+$ CTLs from naive or CML-bearing mice

993 treated with PBS or DT overnight in a 1:1 ratio, followed by plating in methylcellulose. Myeloid
994 CFU and re-plating capacity in vitro (n=3 mice/group); One-way ANOVA followed by Tukey's
995 post-test. **(H)** Perforin (*Prf1*), **(I)** Granzyme A (*GrzmA*) and **(J)** Granzyme B (*GrzmB*) mRNA
996 expression levels in BM $CD8^+$ CTLs measured by qPCR. Data are normalized to *Gapdh* (naive:
997 n=4 mice; CML: n=5 mice; CML DT: n=4 mice); One-way ANOVA followed by Tukey's post-
998 test. Data are displayed as mean±SEM. Statistics: * $P<0.05$, ** $P<0.01$, *** $P<0.001$ and ****
999 $P<0.0001$. Dotted line represents the time point experiment termination day 90.
1000

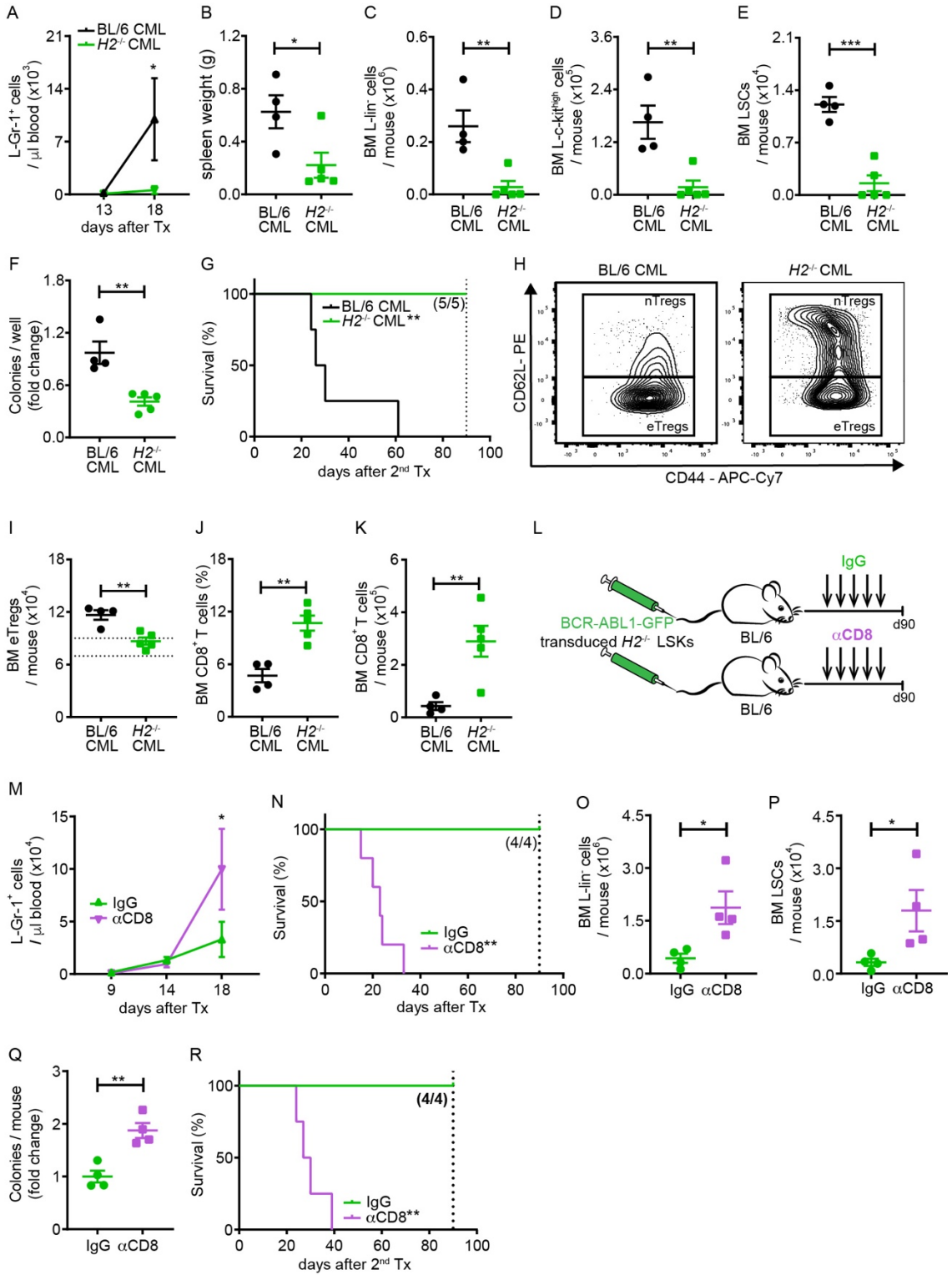

Figure 6: Tregs in the BM of CML mice are activated through interaction with MHC class II on leukemia cells resulting in immune escape of LSCs. (A) L-Gr-1^{+} cells in blood from BL/6 and MHC class II-deficient $(H2^{-/-})$ CML mice (n=4-5 mice/group); Two-way ANOVA followed by Sidak's multiple comparison test. **(B-E)** Spleen size, numbers of **(C)** L-lin^{-}, **(D)** L-c-kit^{high} cells and **(E)** LSCs in BM and **(F)** Colony formation capacity per mouse of BL/6 and

H2$^{-/-}$ CML mice (18 day); Student t-test. **(G)** BM cells of primary CML mice (day 18) were injected i.v. into lethally irradiated secondary BL/6 recipients and survival was monitored; log-rank test. **(H)** Gating strategy to identify nTregs and eTregs; pre-gated on CD4^{+} Foxp3^{+} Tregs. **(I)** Numbers of eTregs within CD4^{+} T cell population in BL/6 and *H2*$^{-/-}$ CML. Dotted lines: range of eTregs observed in naive mice (n=5); Student t-test. **(J)** Frequencies and **(K)** numbers of CD8^{+} T cells in BL/6 and *H2*$^{-/-}$ CML mice (day 18); t-test. **(L)** BL/6 mice were treated i.p. with an αCD8 mAb (75µg/injection) or control IgG at days -2, -1, 4, 9 and 14 (Groups: IgG: n= 4, αCD8: n=5 mice/group). **(M)** Number of L-Gr-1^{+} cells in the blood and **(N)** Kaplan-Meier survival graph of IgG- or αCD8-treated *H2*$^{-/-}$ CML mice (Groups: IgG: n= 4, αCD8: n=5 mice/group); Two-way ANOVA followed by Sidak's multiple comparison test and log-rank test**. (O)** Number of L-lin^{-} cells and **(P)** LSCs in the BM and **(Q)** Colony formation capacity per mouse of IgG-treated and αCD8-treated *H2*$^{-/-}$ CML mice (day 16; n=4 mice/group); t-test. **(R)** Kaplan-Meier survival graph from mice receiving BM cells of primary CML mice (day 16; n=4 mice/group); log-rank test. Data are displayed as mean±SEM. * P<0.05, ** P<0.01, and *** P<0.001. Dotted lines: time point experiment termination day 90.

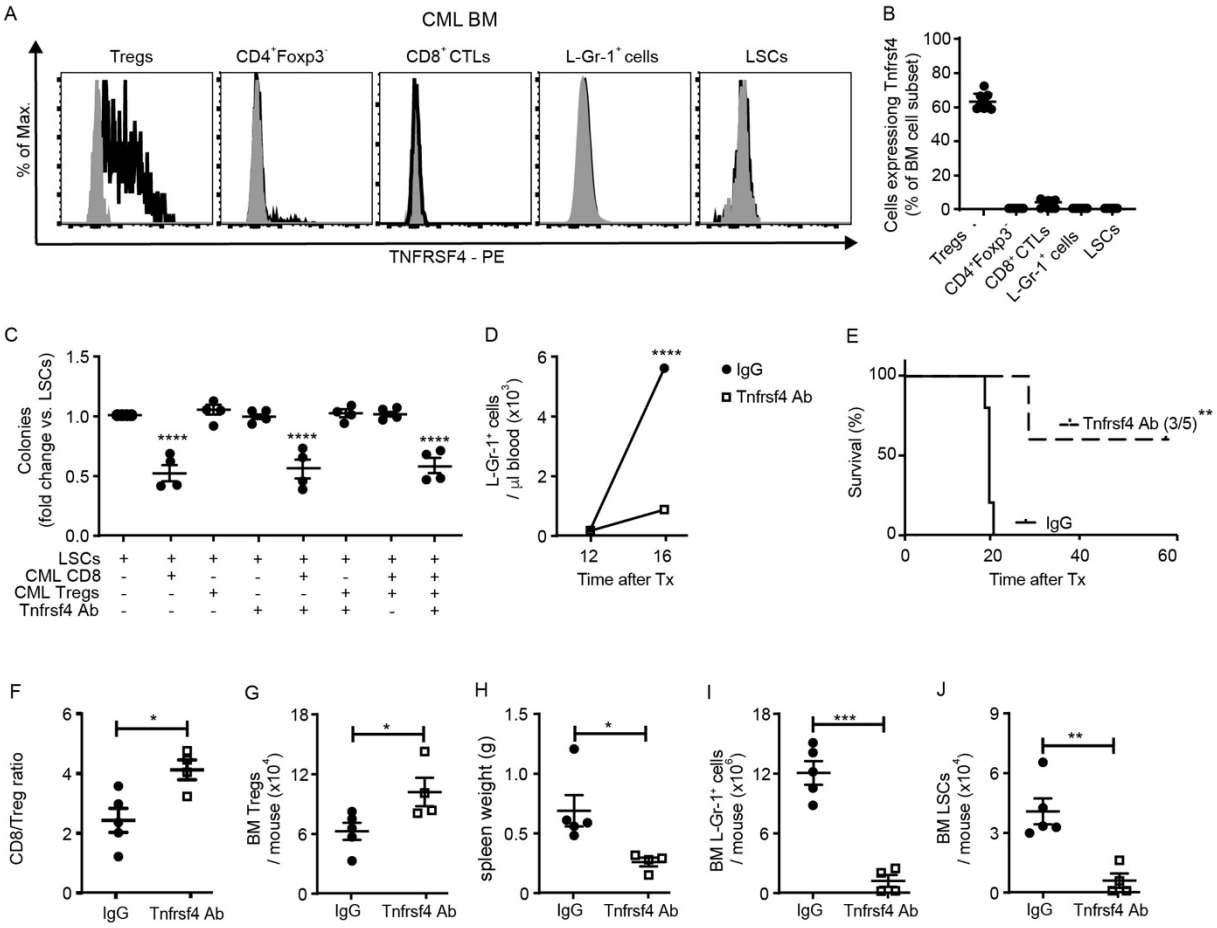

Figure 7: Stimulation of Tnfrsf4-signaling reduces the capacity of Tregs to protect LSCs from CD8$^+$ CTL-mediated killing. (A) Representative FACS plots for the expression of Tnfrsf4 on CD4$^+$Foxp3-GFP$^+$ T cells (Tregs), CD4$^+$Foxp3$^-$ T cells, CD8$^+$ CTLs, L-Gr-1$^+$ cells and LSCs in the BM of *Foxp3*^{DTR} CML mice. One representative out of 9 plots is depicted. Staining: black; isotype control: grey. **(B)** Frequency of CD4$^+$Foxp3-GFP$^+$ T cells, CD4$^+$Foxp3$^-$ T cells, CD8$^+$ CTLs, L-Gr-1$^+$ cells and LSCs in the BM of CML mice expressing Tnfrsf4 (n=9 mice/cell subset). **(C)** LSCs from the BM of *Foxp3*^{DTR} CML mice were cultured with BM CD8$^+$ T cells and/or BM Tregs of the same mice pre-treated for 2h with a Tnfrsf4 antibody (clone OX-86, 30 µg/ml) or respective control antibody at a ratio of 1:1:1 in triplicates followed by plating in methylcellulose. Colonies were enumerated 7 days later; One-way ANOVA followed by Tukey's post-test. **(D, E)** BL/6 CML mice were randomized to control IgG or anti-Tnfrsf4 antibody treatment (OX-86, 200 µg/mouse, i.p, for six times every second day, starting at day 12) and leukemia development and survival was monitored. **(D)** Number of L-Gr-1$^+$ cells in the

blood of IgG-treated and Tnfrsf4 antibody-treated BL/6 CML mice; Two-way ANOVA followed by Sidak's multiple comparison test (n=5 mice/group). **(E)** Kaplan-Meier survival curves of control IgG- and TNFRSF4-Ab treated CML mice (IgG: n=5, Tnfrsf4: n=5); log-rank test. **(F)** CD8/Treg ratio in the BM, **(G)** Treg numbers in the BM, **(H)** spleen weight, **(I)** numbers of L-Gr-1^{+} cells and **(J)** LSCs in the BM of control IgG- and TNFRSF4-Ab treated CML mice (IgG: n=5, Tnfrsf4: n=4) 18 days after CML transplantation. t-test. Data are displayed as mean±SEM. * P<0.05, ** P<0.01, *** P<0.001, and **** P<0.0001. One representative out of two independent experiments are shown.

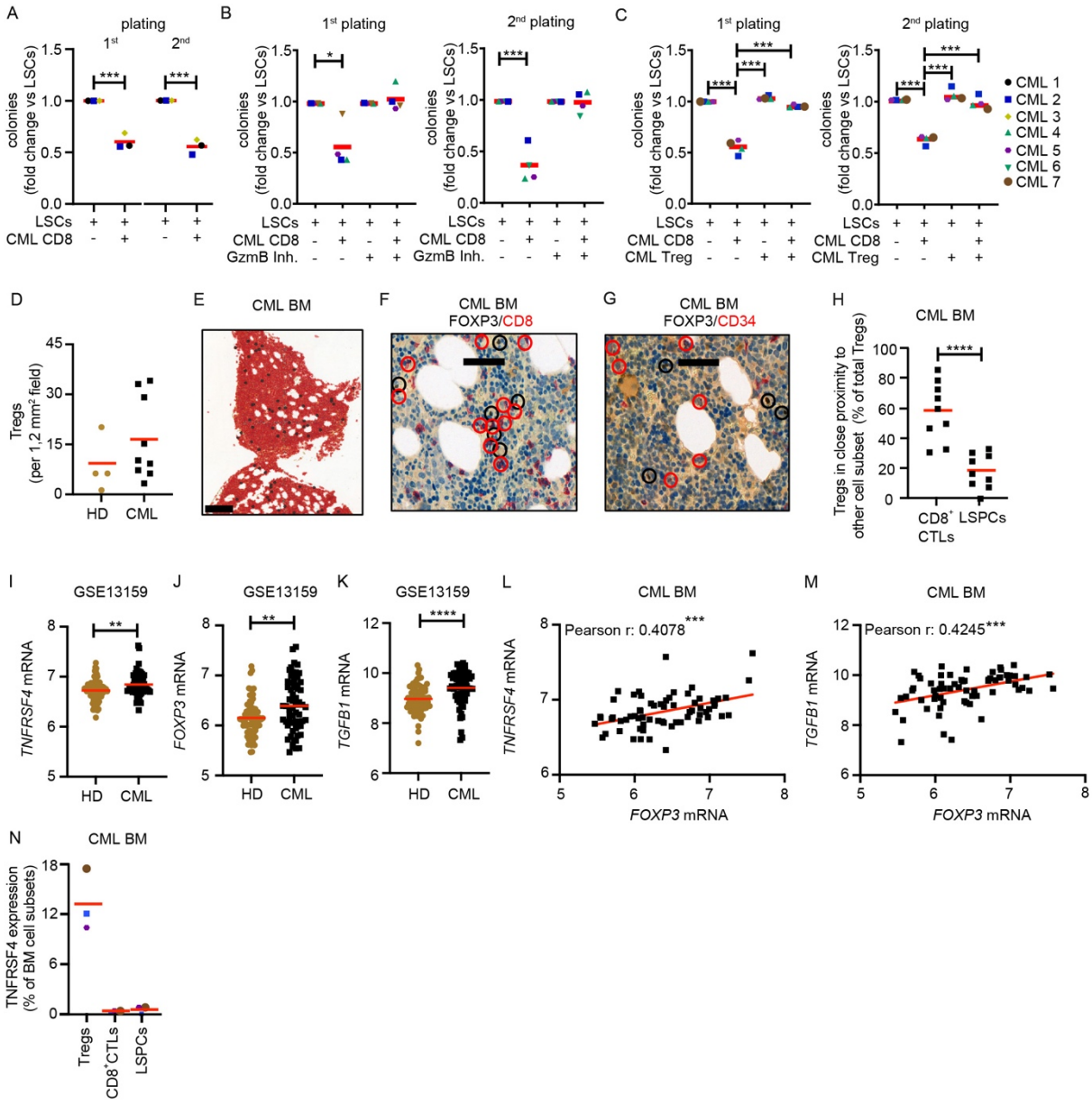

Figure 8: Tregs protect human CD34$^+$CD38$^-$ CML stem/progenitor cells from elimination by CD8$^+$ CTLs. (A) Colony-forming and replating-capacity of CD34$^+$CD38$^-$ LSCs (CML 1-3) cultured overnight in the presence and absence of CD8$^+$ CTLs of the same CML patients at a ratio of 1:1; t-test. **(B)** Colony-forming and replating-capacity of LSCs (CML 4-7) pre-treated with the granzyme B inhibitor 1 (100µM) and cultured in the presence and absence of CD8$^+$ CTLs at a ratio of 1:1 overnight; t-test. **(C)** Colony-forming and replating-capacity of LSCs (CML 4-6) cultured in the presence and absence of CD8$^+$ CTLs and/or CD25$^+$CD127^{lo} CD4$^+$ Tregs at a ratio of 1:1:1. One-way ANOVA followed by Tukey's post-test. **(D)** Numbers of BM Tregs in CML patients and healthy donors (CML: n=10, HD: n=4). Tregs per 1,2mm^2 field were determined; t-tests. **(E)** Distribution of BM FOXP3$^+$ Tregs (scale bar 200µm, n= 10 CML patients). **(F-G)** Spatial localization of BM FOXP3$^+$ Tregs in respect to **(F)** CD8$^+$ CTLs and **(G)** CD34$^+$ CML stem/progenitor cells (LSPCs, scale bar 50 µm, n=10 CML patients; FOXP3: brown; CD8$^+$ CTLs and LSPCs: red). FOXP3$^+$ cells: black; CD8$^+$ CTLs and LSPCs: red circles. **(H)** Frequency of BM Tregs located near CD8$^+$ CTLs and LSPCs (n=10 CML patients). Close proximity was defined as a distance of ≤ two cell nuclei; t-tests. **(I)** *TNFRSF4*, **(J)** *FOXP3* and **(K)** *TGFB1* mRNA expression in CML patients and healthy donors (HD, n=73; CML: n=76; GSE13159); t-test. **(L, M)** Correlation of *FOXP3* with **(L)** *TNFRSF4* and **(M)** *TGFB1* mRNA expression in BM of CML patients (n=76; GSE13159); Spearman correlations. **(i)** Frequency of CD25$^+$CD127^{lo} CD4$^+$ Tregs, CD8$^+$ CTLs and LSPCs expressing TNFRSF4 on the cell surface in CML patients (CML 2, 5, 7) analyzed by FACS. Data are displayed as mean. * P<0.05, ** P<0.01, *** P<0.001 and **** P<0.0001.